


Research Article

Holocene paleohydrology from alpine lake sediment, Emerald Lake, Wasatch Plateau of central Utah, USA

Lesleigh Anderson^{1*} , Gary Skipp¹, Laura Strickland¹, Jeff Honke¹, Jeremy Havens¹ and D. Paco VanSistine¹

¹U.S. Geological Survey Geoscience and Environmental Change Science Center, Denver CO

Abstract

Holocene sediments at Emerald Lake in central Utah (3090 m asl) document the paleohydroclimatic history of the western Upper Colorado River headwater region. Multi-proxy analyses of sediment composition, mineralogy, and stable isotopes of carbonate ($\delta^{18}\text{O}$ and $\delta^{13}\text{C}$) show changes in effective moisture for the past ca. 10,000 years at millennial to decadal timescales. Emerald Lake originated as a shallow, closed-basin cirque pond during the Early Holocene. By ca. 7000 cal yr BP, higher lake levels and carbonate $\delta^{18}\text{O}$ values indicate rising effective moisture and higher proportions of summer precipitation continued at least until ca. 5500 cal yr BP when a landslide entered the lake margin. Between ca. 4500 and 2400 cal yr BP dry conditions at Emerald Lake envelop the timing of the ‘Late Holocene Dry Period’ identified at lower elevations. For the past ca. 2500 years, Emerald Lake $\delta^{18}\text{O}$ values were relatively low, indicating wetter conditions and higher snow input (compared to rain), except for dry periods at ca. 2000 cal yr BP and during the Medieval Climate Anomaly at ca. 1000 and ca. 500 cal yr BP. Results provide a long-term perspective on precipitation extremes that influence regional water supplies from a snow-dominated catchment typical of the predominant source region for the Upper Colorado River.

Keywords: Holocene, Paleohydrology, Lake level, Carbonate oxygen isotopes, Upper Colorado, High elevation lake, Great Basin

(Received 29 March 2022; accepted 18 July 2022)

INTRODUCTION

Historic droughts in the intermountain region of the Rocky Mountains, including the Upper Colorado River Basin (UCB), are fueled by reductions in snowpack, which is the region’s primary water source. The historical record highlights the need for Holocene perspectives on precipitation extremes and drought (defined as meteorological drought, e.g., Mishra and Singh, 2010). In the continental interior of the American west, the seasonal interplay between atmospheric flow patterns (i.e., the jet stream) with geographic mechanisms and topography leads to winter maxima in the annual distribution of precipitation and higher precipitation amounts at higher elevation (Bryson and Hare, 1974; Redmond, 2003; Shinker et al., 2006; Shinker and Bartlein, 2011). Mountain snowpack is of fundamental importance for water supply because it contributes most of the water for storage and use downstream. However, low elevation locations, including pluvial lakes, constitute the majority of the Late Pleistocene records that provide the framework for our current understanding of the paleohydrologic history of the region (Thompson et al., 1993; Bartlein et al., 1998; Madsen et al., 2001; McGee et al., 2012; Reheis et al., 2014; Oviatt, 2015; Thompson et al., 2016).

There is an important distinction between the paleohydrology of high elevation locations where most water is supplied versus low elevation locations where most water is used. Redmond (2003) identified the complex relationship between lower elevation surface water amounts and mountain snowpack by recognizing that peak snowmelt during spring runoff is brief, and commonly occurs before peak ecological water use during summer growing seasons when rainfall is infrequent and sporadic. Compared to high elevations, intermountain valley geographies have relatively warmer temperatures and lower annual precipitation amounts, and are frequently characterized as semi-arid. This can lead to unique proxy sensitivity to wet and dry conditions by comparison with nearby alpine areas (Wahl et al., 2015; Munroe and Laabs, 2020; Quirk et al., 2020). Records of regional water supply, at its primary source, can be found at high elevation, snowfall-dominated locations using a precipitation sensitive proxy such as water isotope tracers from lake sediments.

Lakes are natural reservoirs of mixed surface and meteoric waters, and stable isotope ratios are widely used to study hydrologic and hydroclimatic processes, past and present (Gibson et al., 2016; Horton et al., 2016). Lake water isotopes of oxygen and hydrogen, $\delta^{18}\text{O}$ and $\delta^2\text{H}$, respectively, reflect processes related to water source and evaporation. Source waters reflect the isotope values of precipitation, including that which falls directly on a lake’s surface combined with surface and groundwater inflow (Shapley et al., 2008). Source water isotope values are affected by precipitation amount, atmospheric vapor source and trajectory, and the temperature of condensation (Friedman 2002a,

*Corresponding author email address: <land@usgs.gov>

Cite this article: Anderson L, Skipp G, Strickland L, Honke J, Havens J, VanSistine DP (2023). Holocene paleohydrology from alpine lake sediment, Emerald Lake, Wasatch Plateau of central Utah, USA. *Quaternary Research* 112, 1–19. <https://doi.org/10.1017/qua.2022.42>

© University of Washington. Published by Cambridge University Press, 2022. This is a work of the U.S. Government and is not subject to copyright protection in the United States. This is an Open Access article, distributed under the terms of the Creative Commons Attribution licence (<https://creativecommons.org/licenses/by/4.0/>), which permits unrestricted re-use, distribution, and reproduction in any medium, provided the original work is properly cited.

2002b; Smith, 2002). Evaporation from a lake's surface causes preferential loss of the light isotope ^{16}O , causing a relative increase in the heavy isotope ^{18}O , leaving higher $\delta^{18}\text{O}$ values in the remaining lake water. There is greater potential for evaporation with extended lake water residence times, which is a function of lake hydrology that can be characterized by modern water isotope values (e.g., Smith and Palmer, 2012). The range of modern isotope values provides the framework for interpretation of past lake water isotope variations found in sediment records, such as those derived from lake carbonate deposits (e.g., Anderson et al., 2016a).

Most existing lake water isotope sediment records of the intermountain west are from low-elevation environments, including Walker and Pyramid lakes in Nevada (Benson et al., 2002; Lund et al., 2021), Owens Lake and Mono Lake in California (Li et al., 1997; Menking et al., 1997), and Bear Lake in Idaho-Utah (Bright et al., 2006; Dean et al., 2007). Holocene studies include Foy, Jones, and Crevice lakes in Montana (Stevens et al., 2006; Stevens and Dean, 2008; Shapley et al., 2009; Whitlock et al., 2012), San Luis Lake in central Colorado (Yuan et al., 2013), and Lower Pahranaagat Lake in southern Nevada (Theissen et al., 2019). High elevation lake records are relatively uncommon in Utah (Munroe and Laabs, 2020), and those focused on carbonate $\delta^{18}\text{O}$ are currently limited to northwestern Colorado at Bison and Yellow lakes, 3255 m and 3140 m elevation, respectively (Anderson, 2011, 2012). Located in the eastern Upper Colorado River Basin (UCB), the Bison and Yellow records characterize precipitation at multidecadal-scale resolution to provide regional Holocene snowpack trends (Anderson et al., 2016b). Additional high elevation carbonate $\delta^{18}\text{O}$ records are needed to evaluate patterns and processes related to seasonal precipitation, temperature, evapotranspiration, infiltration, and runoff across the sub-regions of the UCB that have yet to be explored by paleoclimatic investigations.

This study presents a new lake carbonate $\delta^{18}\text{O}$ paleoclimate record for the Holocene from Emerald Lake in central Utah (Fig. 1). At 3090 m elevation, the headwater lake is on the summit of the Wasatch Plateau, which delineates the border between the Great Basin and Colorado Plateau regions. The location of Emerald Lake on the western boundary of the UCB provides a new opportunity to evaluate sub-regional snow and drought patterns within the watershed. We show that the multi-decadal scale $\delta^{18}\text{O}$ record (ca. 30-year average resolution) from Emerald Lake reflects changes in precipitation and evaporation by utilizing a modern lake $\delta^{18}\text{O}$ interpretive framework, and multiproxy sediment variations provide evidence for changes in lake level. Comparison with records from the eastern Great Basin and northern Rockies approximates the geographic scale of synoptic climate patterns related to jet stream and North American Monsoon (hereafter 'monsoon') dynamics. With this context in mind, four questions are addressed by this study. (1) Were Holocene paleohydrologic trends consistent at high and low elevations? (2) Were paleohydrologic extremes in the Upper Colorado typically basin-wide or were sub-regional variations common? (3) Is there evidence for regional precipitation patterns with spatial dipole characteristics (e.g., wet north and dry south) and/or time-transgressive patterns that bear resemblance to historical patterns? (4) How common are non-analogue conditions?

The Wasatch Plateau has a long history of damaging landslides, including mass movement that evidently has altered the western margin of Emerald Lake (DeGraff, 1978; McDonald and Giraud, 2015). The primary mechanism for historic slope

instability is soil saturation caused by either high snowmelt runoff or intense rainfall events (Fleming et al., 1988; Baum and Fleming, 1989). Alternatively, Holocene landslides may have also been triggered by seismic activity on steep normal fault segments of the Wasatch fault complex that cross the plateau, including the Emerald Lake watershed (Machette et al., 1991; Witkind et al., 2006; DuRoss et al., 2016). The radiocarbon-based chronology of the Emerald Lake sedimentary record provides accurate timing for a landslide event and allows evaluation of its occurrence within the context of the paleoclimatic record.

STUDY SITE

Emerald Lake (39.0738°N, 111.4977°W, 3090 m asl) is a headwater of the North Fork of Muddy Creek, a tributary of the Dirty Devil, Fremont, and Upper Colorado rivers (Fig. 2) in the Manti-La Sal National Forest, and is located within the early Paleogene Flagstaff Formation, which is a lacustrine deposit within the Sevier foreland basin that consists of limestones, mudstones, minor sandstones, and evaporites (Bowen et al., 2008). The limestones are locally dolomitic. During the Pleistocene, the Wasatch Plateau was glaciated (Spieker and Billings, 1940; Larson, 1996; Witkind et al., 2006). Early Holocene and Late Pleistocene megafaunal remains discovered in glaciolacustrine sediments include Columbian mammoth, mastodon, short-faced bear, horse, and bison (Miller, 1987; Gillette and Madsen, 1992, 1993).

The east side of the plateau crest is scalloped by glacial cirques, including the Emerald Lake basin, indicating ice accumulation related to wind-blown snow (e.g., Dohrenwend, 1984). Based on Larson's (1996) mapping of surface moraines, the basin's cirque glaciers were ~2 km in longitudinal extent, and the lake is naturally impounded by a ridge of Pleistocene till ~3 m higher than the modern lake (Fig. 2). The lake is primarily spring fed (i.e., a few minor ephemeral inflow streams occur and there is no surface outflow). A normal fault extends north-south across the Emerald Lake basin. The fault trace is located east of the lake, ~40 m lower than the lake surface, where a spring discharges. Witkind et al. (2006) mapped the fault, which crosscuts the left and right lateral moraines, and observed no offsets. However, offset is clear where the fault intersects the west-facing slopes of Block Mountain near a landslide toe. On the north-facing slope of Block Mountain, a landslide postdates the right-lateral moraine. If the landslides were triggered by fault movement, the fact that a slide buried the moraine may indicate post-glacial and potentially Holocene seismic activity, as described for Wasatch Fault segments to the north (Machette et al., 1991; DuRoss et al., 2016).

Emerald Lake has a surface area of 0.032 km², a watershed area of 0.412 km² (watershed-to-lake area ratio of 12.8), and a maximum depth of 8 m in a flat central area. Shallow littoral areas of <2 m water depth occur along the southern margin and along portions of the western shoreline near the landslide that moved down the east-facing cirque (Fig. 3A). Where the landslide toe is submerged, it slopes steeply downward towards the lake's depocenter. Shallow margins to either side indicate that a landslide overran what was a continuous shallow area, thereby reducing the surface area of the lake (Fig. 3B).

The sediments of Emerald Lake reflect the basin's watershed and limnology. The water column is thermally and chemically stratified during the summer, and biologically mediated endogenic calcite precipitates within the alkaline and calcium-saturated epilimnion. Thus, sediments at water depths within

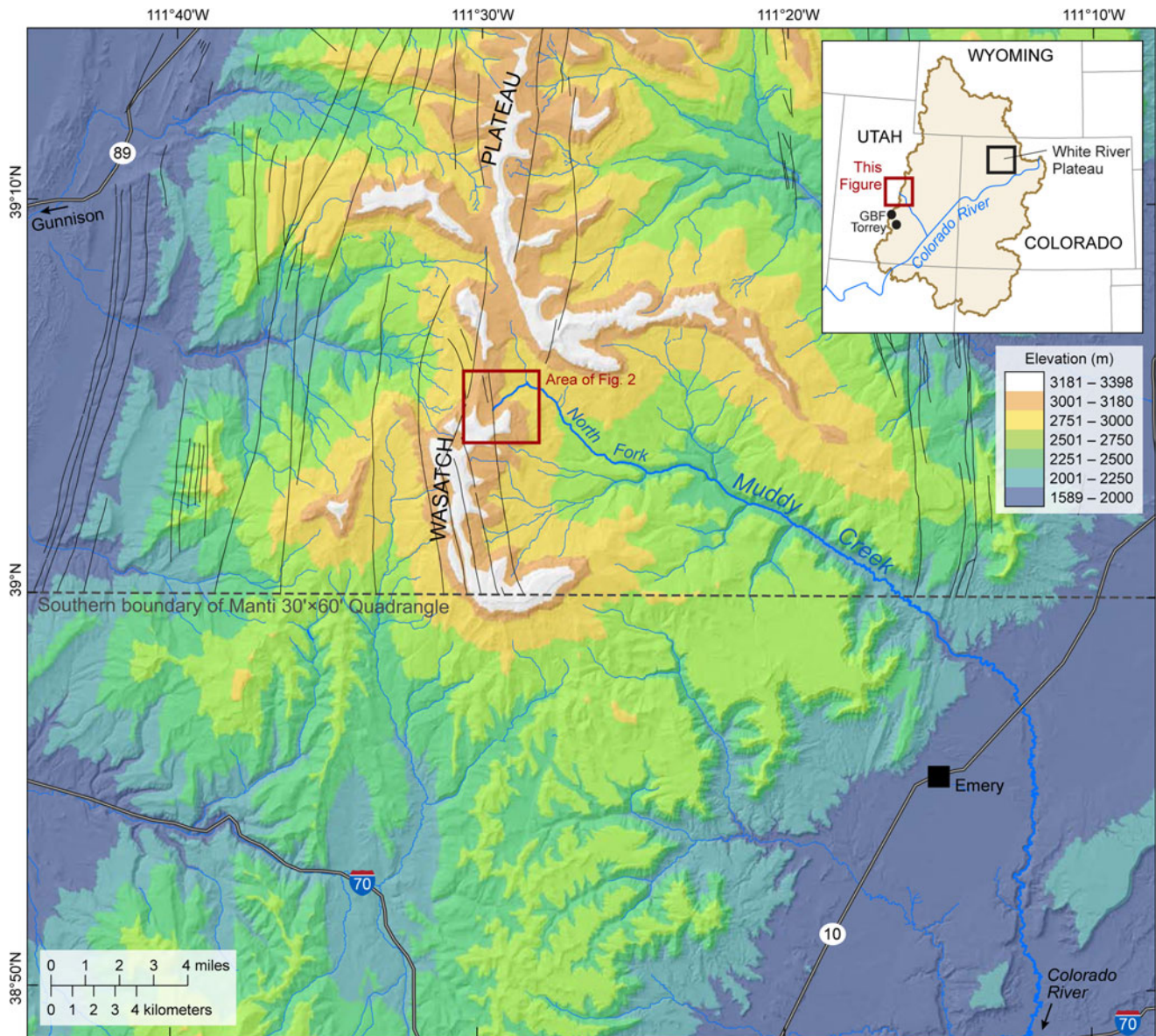


Figure 1. Map of the Emerald Lake study area (red box) within the Muddy Creek watershed in the southern Wasatch Plateau, central Utah, on a colored digital elevation model. The inset shows the area's location in the Upper Colorado River Basin (UCB) in relation to the White River Plateau in northwest Colorado, Garden Basin Fen (GBF) and Torrey soils, discussed in the text. North-south normal faults (black lines) were mapped by Witkind et al. (2006) and are shown for the area only within the U.S. Geological Survey Manti 30'x 60' quadrangle.

the epilimnion contain abundant well-preserved carbonates, but carbonate dissolution during settling within the water column limits the abundance at epilimnetic depths. Allochthonous sediments weathered from the Flagstaff Formation include mudstones, sandstones, calcite, and dolomite. Thus, these detrital sediments are known to have distinct palustrine Flagstaff carbonate stable isotopic values that were influenced by early Paleogene greenhouse climates in addition to paragenesis effects (Bowen et al., 2008). The detrital carbonates differ in mineralogy and isotopic values from endogenic carbonates, therefore they can be quantified and accounted for in the isotope record.

Vegetation on the summit of the Wasatch Plateau is a mosaic of open grasslands, tundra species, and fragmented stands of mature Engelmann spruce and Douglas fir (*Picea engelmannii* and *Pseudotsuga menziesii*, respectively), with lesser occurrence of ponderosa pine (*Pinus ponderosa*). Local ecosystem dynamics

are driven by fire and insect outbreaks as well as weather extremes and herbivory. The extensive Englemann spruce mortality in the Emerald Lake watershed that is evident today (Fig. 3C) mostly occurred in 1986 and 1998 during two historical spruce beetle (*Dendroctonus rufipennis*) outbreaks, which affected the entire Wasatch Plateau area (Dymerski et al., 2001). Previous severe disturbance of the landscape occurred during late nineteenth century logging (Morris et al., 2010), and dynamic fire regimes have influenced the landscape throughout the Holocene (Morris et al., 2015).

Climate of the Wasatch Plateau is significantly wetter and colder than elevations below 2000 m. We obtained the 30 yr climate normal (1980–2010) from the Parameter-elevation Regressions on Independent Slopes Model (PRISM) for Emerald Lake (3090 m asl). Mean annual precipitation ranges from 90–100 cm and mean annual temperatures are between -4°C and

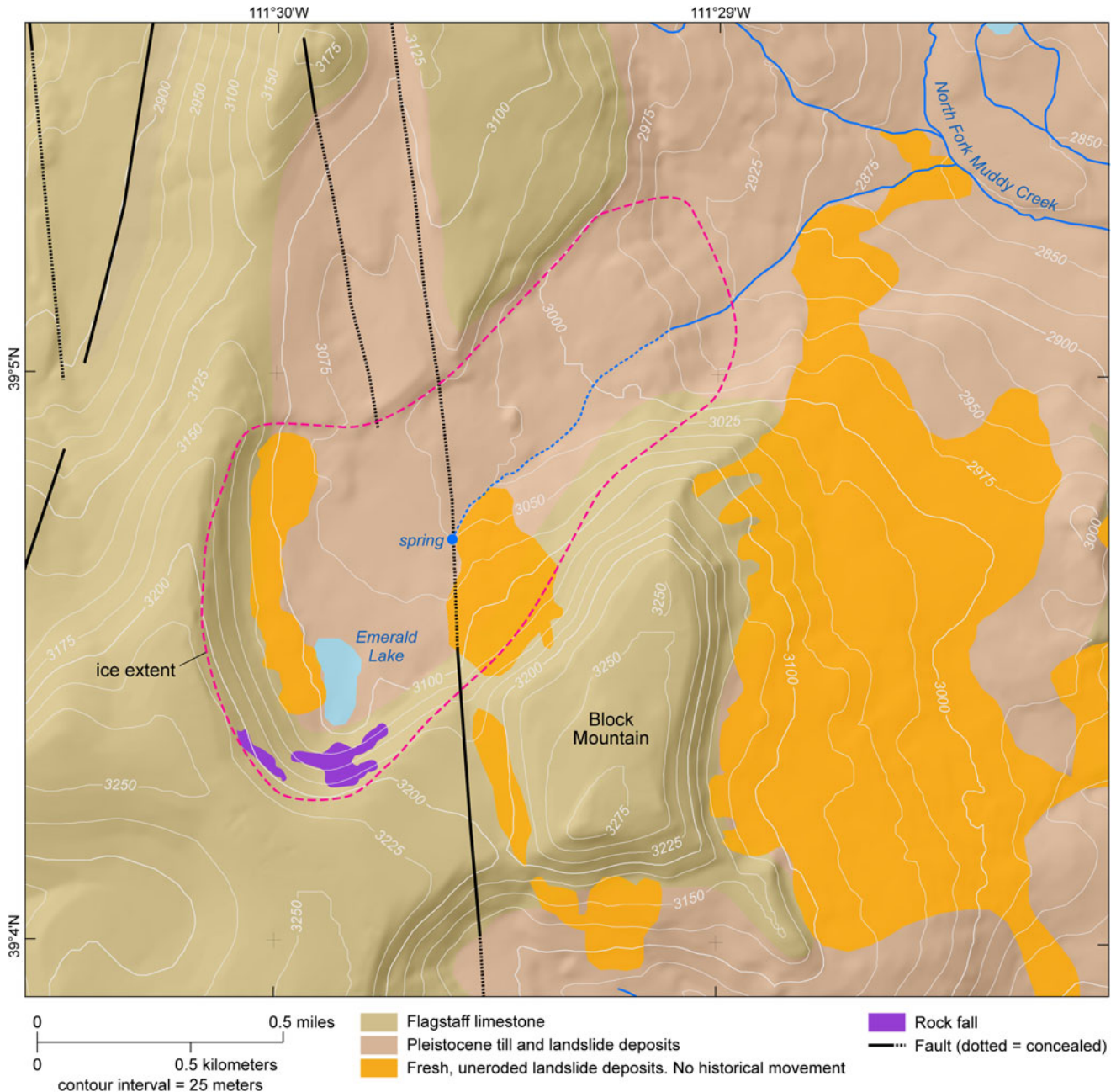


Figure 2. Expanded view of study area from Figure 1 of the Emerald Lake watershed with topography and surface water, ice-extent (Larson, 1996), faults and geologic units (Witkind et al., 2006), landslides (orange), and rockfall (purple) (McDonald and Giraud, 2015).

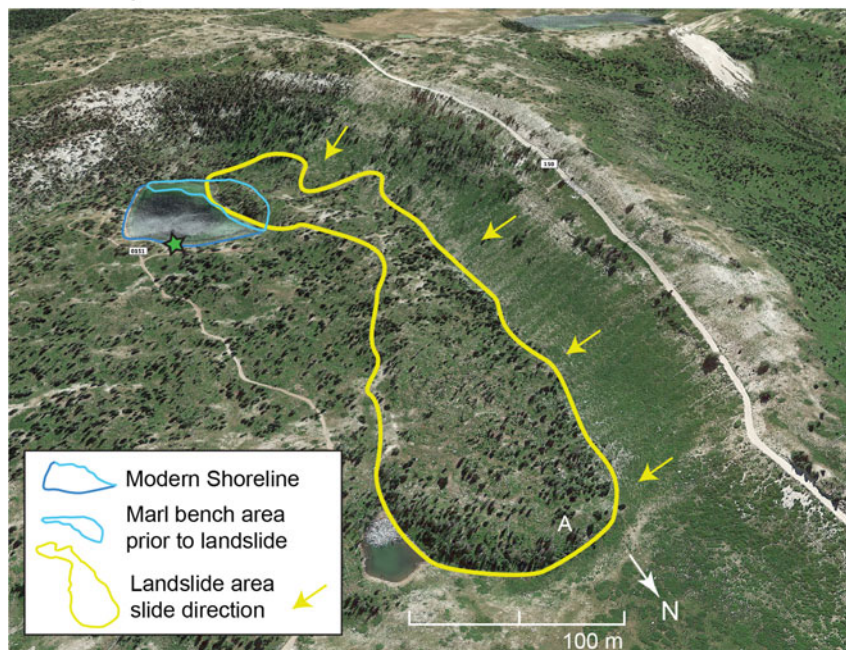
–2°C (PRISM Climate Group, 2018). The seasonal distribution of precipitation is strongly biased by winter, with snowfall accounting for ~70% of the annual total and monthly maximums in precipitation occurring between February and April (Mock and Birkeland, 2000). Peak snowmelt runoff begins in early May and concludes by mid-to-late June. Snow water equivalent (swe) values in the Emerald Lake area range from 18–68 cm, with a median of ~30 cm, based on data from the United States Department of Agriculture (USDA) National Resource Conservation Service (NRCS) high elevation snowpack telemetry (SNOTEL) Dill’s Camp site (2795 m elevation, 1978 to present). Using a snow-to-liquid ratio of 10:1, these swe values yield snowfall depths from ~2–7 m, although higher snow-to-liquid ratios

and snow depths commonly occur. While summer precipitation may be associated with northern or western frontal boundaries, it most regularly occurs as intense convection events associated with southerly upper level moisture that is usually related to monsoon dynamics (Adams and Comrie, 1997; Higgins et al., 1998).

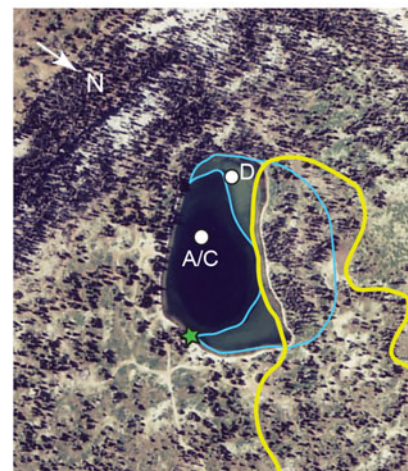
METHODS

Emerald Lake sediment cores were retrieved in August 2006 from a securely anchored floating platform with a modified Livingstone piston corer at two sites—designated core A/C at 8 m water depth,

A. Oblique



B. Overhead



C. Ground view

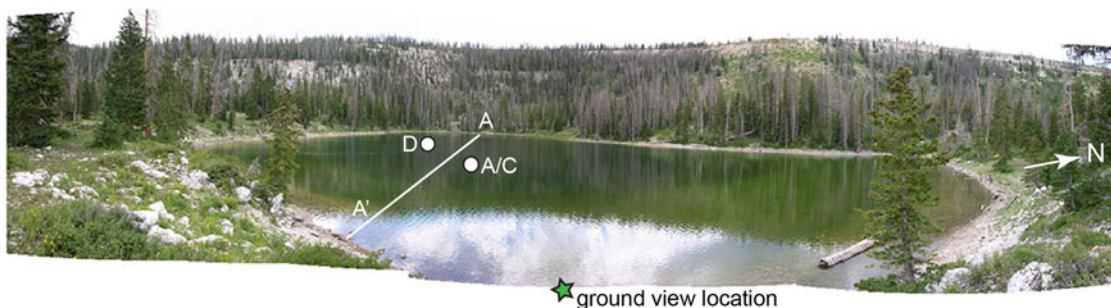


Figure 3. Emerald Lake imagery. (A) Oblique view (Digital Globe), (B) overhead (aerial photography), and (C) ground view and core locations A/C and D (photo credit, Lesleigh Anderson). The modern shoreline in (A) is outlined in dark blue. The landslide into the lake is outlined in (A) and (B) with yellow, and the inferred pre-landslide extent of the shallow marl bench is outlined in light blue. The location of the ground view is shown by a green star in (A) and (B). The transect A-A' refers to the schematic block diagram in Figure 9.

and core D at 1.45 m water depth. Core A/C is a 300 cm long composite from the central basin reported by Morris et al. (2015) that includes analyses of pollen, charcoal, and radiocarbon of terrestrial plant macrofossils. For this study, core A/C samples were obtained for dry bulk density at continuous 1-cm increments ($n = 296$). Percent organic and inorganic carbon was determined from dry, pulverized sub-samples using total carbon (TC) and total inorganic carbon (TIC) measurements from a UIC Inc.TM CO₂ coulometer (Engleman et al., 1985). Percent organic carbon was calculated as the difference between TC and TIC. Percent organic matter (%OM) was calculated as 2.5 times TOC, an approximation based upon the molar fraction of carbon in organic hydrocarbons. Percent carbonate was calculated as $TIC / 0.12$, where 0.12 is the molar fraction of carbon in CaCO₃. The accuracy and precision for both TC and TIC is 0.1%, as determined by sample runs and internal standards.

Shallow water core D consists of five overlapping sections, including the undisturbed sediment-water interface, which was extruded in the field at 0.5-cm increments to 56 cm depth

(Glew et al., 2001). Overlapping core D sections were correlated based on visual and physical properties to produce a composite core of 250 cm length. After taking whole core magnetic susceptibility measurements of the core sections at 1-cm increments with a BartingtonTM susceptibility meter, all sections were split, photographed, and visually logged for biogenic features, sedimentary structures, composition, and Munsell color. Contiguous samples were obtained at 1.0-cm increments for dry bulk density and carbon analyses.

Core D carbonate isotope analyses were conducted on contiguous 1-cm samples ($n = 249$), as described below. The macroscopic carbonate particles identified include charophyte stem encrustations, ostracode valves, gastropods, and bivalve shells and fragments. Microscopic carbonate grains were identified as calcite and dolomite using Scanning Electron Microscopy (SEM) and Energy Dispersive Spectroscopy (EDS). To separate the fine-grained bioinduced carbonates from larger biological and allochthonous particles, samples were wet sieved through nested screens (250, 125, 63, 32 μm), collected separately, and

freeze-dried. The finest fractions, either the <32 μm size, or the <32 μm size combined with the 32–63 μm sizes (if the <32 μm sample was of insufficient mass by itself), were visually examined for purity and powdered before subsampling for CO_2 extraction by a Kiel automated device coupled with a Finnigan Delta 252 isotope ratio mass spectrometer. Calcite oxygen and carbon isotope ratios are reported in per mil (‰) as the relative isotope-ratio difference from the international standard VPDB defined by two equations.

$$\delta^{18}\text{O}_{\text{CaCO}_3} = ([^{18}\text{O}/^{16}\text{O}]_{\text{CaCO}_3}/[^{18}\text{O}/^{16}\text{O}]_{\text{VPDB}}) - 1$$

and

$$\delta^{13}\text{C}_{\text{CaCO}_3} = ([^{13}\text{C}/^{12}\text{C}]_{\text{CaCO}_3}/[^{13}\text{C}/^{12}\text{C}]_{\text{VPDB}}) - 1$$

Determined analytical uncertainties are $\pm 0.05\text{‰}$ and 0.1‰ for oxygen and carbon, respectively, and analyses of random replicate samples fell within the range of analytical error.

Core D mineralogy was determined for samples at 2-cm increments ($n = 151$) by semi-quantitative X-ray diffraction (XRD) techniques (Moore and Reynolds, 1989). Each sample was packed into an aluminum holder and scanned from 15–50° 2θ at 2° 2θ /min using Ni-filtered, Cu-K α radiation at 45 kV, 30 ma with peak intensities recorded as counts per second (cps). Mineral identification used automated peak-search, and peak areas were quantified against standards. Results were obtained as the peak intensity of the main XRD peak for each mineral and reported as a percentage of the sum of the main XRD peak intensities of all minerals. To improve raw XRD mineral percentage precision for the carbonate minerals of foremost interest here, the XRD data were normalized to coulometric TIC following equations in Shapley et al. (2009).

Near-surface lake-water samples obtained for chemistry and isotope analyses were taken in 100 ml and 30 ml HDLP Nalgene™ bottles. Isotope samples were sealed with no head space, and water chemistry samples were unfiltered and acidified. Lake-water anion, cation, and alkalinity analyses were conducted on unfiltered samples at the USGS Colorado Water Science Center using standard methods for inductively coupled plasma atomic emission spectrometry, ion exchange chromatography, and gran titration by an automatic titrator. Detection limits for all species are >0.015 mg/L. Water samples were prepared for oxygen and hydrogen isotopes by automated constant temperature equilibration with CO_2 , and automated H/D preparation by chromium reduction, coupled to an isotope ratio mass spectrometer. Water isotope results are reported in per mil (‰) as the relative difference of isotope ratios (δ) from the international measurement standard Vienna Standard Mean Ocean Water (VSMOW) defined by two equations.

$$\delta^{18}\text{O}_{\text{H}_2\text{O}} = ([^{18}\text{O}/^{16}\text{O}]_{\text{H}_2\text{O}}/[^{18}\text{O}/^{16}\text{O}]_{\text{VSMOW}}) - 1$$

and

$$\delta^2\text{H}_{\text{H}_2\text{O}} = ([^2\text{H}/^1\text{H}]_{\text{H}_2\text{O}}/[^2\text{H}/^1\text{H}]_{\text{VSMOW}}) - 1$$

Determined analytical uncertainties are within $\pm 0.5\text{‰}$ and $\pm 0.05\text{‰}$ for hydrogen and oxygen, respectively. Analyses of random replicate samples fell within the range of analytical error. Emerald Lake surface and water column measurements were

collected in August 2006, with a calibrated Eureka Amphibian™ and Manta™ sonde.

The core D chronology is based on 19 AMS radiocarbon measurements of identified plant macrofossils (Table 1). Terrestrial plant macrofossils were not present in sufficient quantities at some stratigraphic levels, so in some cases aquatic plant macrofossils were used. To evaluate lake water ^{14}C reservoir effects, age offsets were determined for two pairs of terrestrial and aquatic samples obtained from the same sediment depths of 152 cm and 170 cm. Aquatic age differences of +480 and +550 ^{14}C years, respectively, provide an average age correction of 515 ^{14}C years, which was subtracted from the ^{14}C ages of only the aquatic samples prior to age calibration. Both measured and calibrated ages (Calib 8.2, IntCal20; Stuiver et al., 2021) are reported and calibrated ages (cal yr BP) are used for discussion. The core A/C chronology by Morris et al. (2015) is based on eight AMS radiocarbon ages, all from terrestrial macrofossils, and no reservoir corrections were applied. The calibrated core A/C ages are updated here using Calib 8.2.1 and the IntCal20 dataset.

RESULTS

Limnology

Water column measurements at the maximum water depth of 8 m were taken in August 2006 and a thermocline was present between 5–6 m depth with the onset of a steep decline in temperatures from surface values of 16.5°C to a low of 9°C (Fig. 4A). Corresponding declines with depth occurred in pH, from 8.94 to 7.13, and dissolved oxygen (DO), from 9.93–2.93 mg/L, whereas specific conductivity (Spc) increased from 97–142 $\mu\text{S}/\text{cm}$. Dissolved strontium (Sr) was relatively high (Table 2). The alkaline (Mg-Ca- HCO_3 -type) waters were determined to be saturated with respect to calcite and aragonite, based on analyses by the Geochemists Workbench v 9.0 program. No aragonite was observed in the sediments by x-ray diffraction; nor were evaporites evident, either in the sediments or along the exposed shorelines examined in 2009, which were dominantly silt and sand-sized silicate grains.

Isotope Hydrology

In 2006 and 2007, Emerald Lake water $\delta^{18}\text{O}$ values were -12.1‰ and -11.1‰ and $\delta^2\text{H}$ values were -98‰ and -94‰ , respectively. These values plot on a local evaporation line (LEL) defined by the regression with a slope of 4.9 based on lakes and spring water collected from nearby lakes on the Wasatch Plateau and other nearby high plateau areas for this study (Fig. 4B; $R^2 = 0.98$; Table S1). Seasonal precipitation isotope values for Utah described by Friedman (2002b) define a local meteoric water line (LMWL) with a slope of 7.7 and $\delta^{18}\text{O}$ range between -2‰ and -20‰ (1991–1996—Brian Head, Cedar City, Delta, Hanksville, and Price; also see Marchetti et al., 2018). The intersection of the LEL with the LMWL and the global meteoric water line (GMWL, slope = 8) provides an estimate for the $\delta^{18}\text{O}$ of mean annual precipitation between -15‰ and -16‰ , which is similar to other regions in the intermountain west with a snow-dominated seasonal precipitation balance (Anderson et al., 2016a). Lake water isotope values along the LEL trajectory away from the intercept reflect progressive enrichment in heavy isotopes (^{18}O and ^2H) in response to evaporation (Gibson et al., 1996). The position of Emerald Lake on the LEL indicates

Table 1. Emerald Lake, Utah, radiocarbon data.

Core Depth (cm)	Material	¹⁴ C Age (¹⁴ C yr BP)	Measured Reservoir Offset	Reservoir Corrected ¹⁴ C Age (¹⁴ C years)	AMS ¹⁴ C Lab # ^c	δ ¹³ C (‰ VPDB)	Median Calibrated Age ^a (Cal yr BP)	1σ range (Cal yr BP)
D07								
0	Core surface	n/a					−57 (AD 2006)	
12	Wood and Picea needle	150 ± 20			CURL-17633	−26	145	9–272
39	Conifer bark	815 ± 15			CURL-12003	−25.6	710	691–729
54	Conifer needles	970 ± 25			CURL-16693	−25	855	801–921
68	Wood	1295 ± 15			CURL-12007	−26.2	1220	1178–1276
97	Conifer cone whole	1745 ± 20			CURL-12011	−22.7	1640	1601–1699
126	Potamogeton Seed	3279 ± 35		2755 ± 35	USGS-1526		2840	2782–2839
139	Picea seedwing fragments	3600 ± 25			CURL-17640	−23.3	3905	3871–3966
152	Conifer bark	4095 ± 20			CURL-12005	−23.4	4595	4528–4785
152	Comparison aquatic	4575 ± 25	480		USGS-1499			
154 ^a	Conifer bark	3865 ± 30			WW-9129	−22.1	4295 ^a	4273–4402
170	Picea needle, wood, charcoal	4770 ± 40			USGS-1500		5520	5476–5580
170	Comparison aquatic	5320 ± 30	550		USGS-1501			
173 ^a	Aquatic	5530 ± 20		5015 ± 20	USGS-1502		5750 ^a	5664–5876
174	Aquatic	5450 ± 30		4935 ± 30	WW-9130	−16	5650	5599–5705
186 ^a	Aquatic	5570 ± 20		5055 ± 20	USGS-1620		5830 ^a	5746–5893
205 ^a	Aquatic	5735 ± 25		5107 ± 25	USGS-1621		5810 ^a	5761–5910
215	Wood	5110 ± 20			USGS-1622		5808	5765–5910
233	Conifer needle Picea?	5685 ± 20			CURL-13023	−21	6460	6411–6490
247	Conifer cone fragments	6140 ± 30			USGS-1338	−25	7040	6953–7155
A/C07 ^b								
0	Core surface						−57 (AD 2006)	
24	²¹⁰ Pb horizon						93	
38	Charcoal	735 ± 15			CURL-18264		680	672–680
67	Charcoal	1280 ± 15			CURL-18248		1230	1177–1271
81 ^a	Conifer needle	2451 ± 271			CAIS-4785		2520 ^a	2424–2695
120	Conifer needle	1617 ± 26			CAIS-4787		1480	1417–1534
154	Conifer needle	2985 ± 24			CAIS-4789		3165	3080–3211
199	Conifer needle	3843 ± 27			CAIS-4791		4250	4156–4345
244	Conifer needle	5381 ± 28			CAIS-4793		6200	6122–6274
284	Conifer needle	8483 ± 26			CAIS-4795		9500	9486–9527

^aNot used in age-depth model.^bFrom Morris et al. (2015) recalibrated with Calib v.8.2.1 (IntCal20) ¹⁴C ages.^cCURL = Institute of Arctic and Alpine Research (INSTAAR) Radiocarbon Laboratory, USGS = USGS Geoscience and Environmental Change Science Center Radiocarbon Laboratory, WW = USGS Reston Radiocarbon Laboratory, CAIS = Univ. of Georgia Center for Applied Isotope Studies.

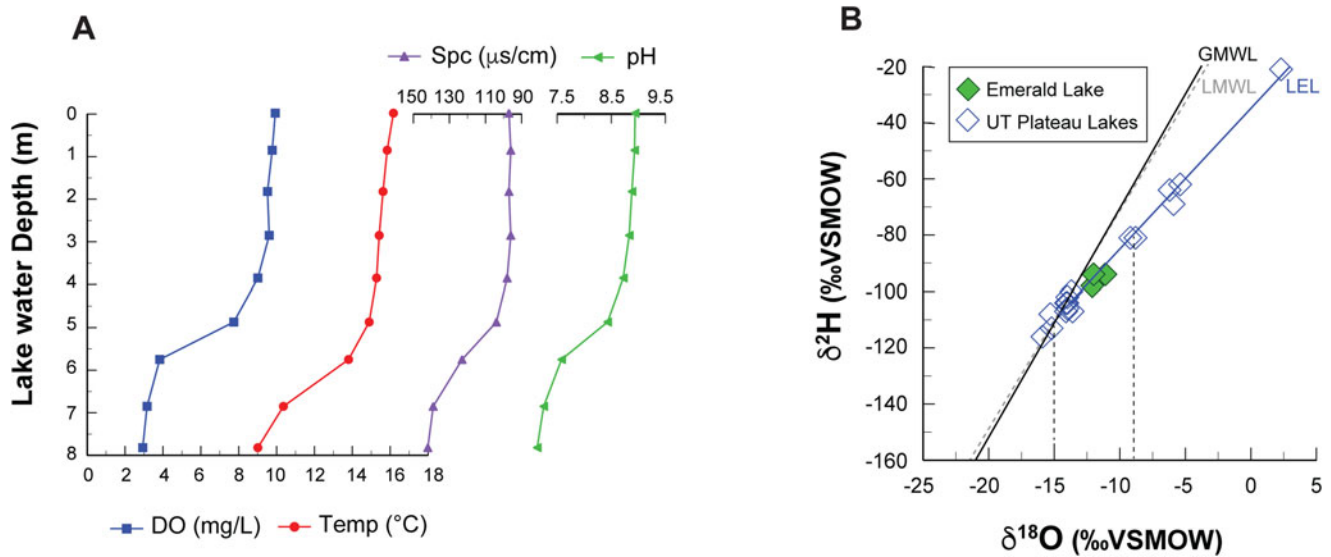


Figure 4. Emerald Lake water column measurements (A) and (B) lake water isotope ratios shown with nearby Utah plateau lakes that form a local evaporation line (LEL) with a lower slope than the global and local meteoric water lines (GMWL, LMWL). The LMWL is by Friedman et al. (2002b). DO = dissolved oxygen; Spc = specific conductivity.

evaporative enrichment of approximately +4‰ for $\delta^{18}\text{O}$, reflecting moderate sensitivity compared to values upwards of ~8‰ at other lakes on the LEL from similar settings. Interannual variations in the $\delta^{18}\text{O}$ values of mean annual precipitation are typically within a smaller range of 2‰ (Friedman, 2002b).

Core lithologies

Core D was divided into four limnic facies based on color, structure, texture, and bulk sedimentary compositions (Fig. 5). From the base of the core moving upwards, Unit I (250–230 cm depth) is composed of faintly bedded, light gray clayey silt.

Aquatic macrofossils include trace amounts of bivalve shells (likely *Pisidium*), *Chara* sp. oogonia, and fine rootlet fragments. *Picea* sp. needles and cone and bark fragments occur near the upper boundary (Fig. S1). The relatively high values of magnetic susceptibility (~1.5 SI) and dry bulk density (0.75 g/cm^3) at the base of the core steadily decline upwards in Unit I as percentages of organic matter (%OM) rise (<5–20%) and inorganic carbonate decline (70–40%).

The transition to Unit II (230–170 cm) is marked by a color shift to light gray olive brown mottled marl with occasional dark olive gray bands. The marl is abundant in herbaceous aquatic material, and contains *Potamogeton* sp. seeds, gastropods,

Emerald Lake core D

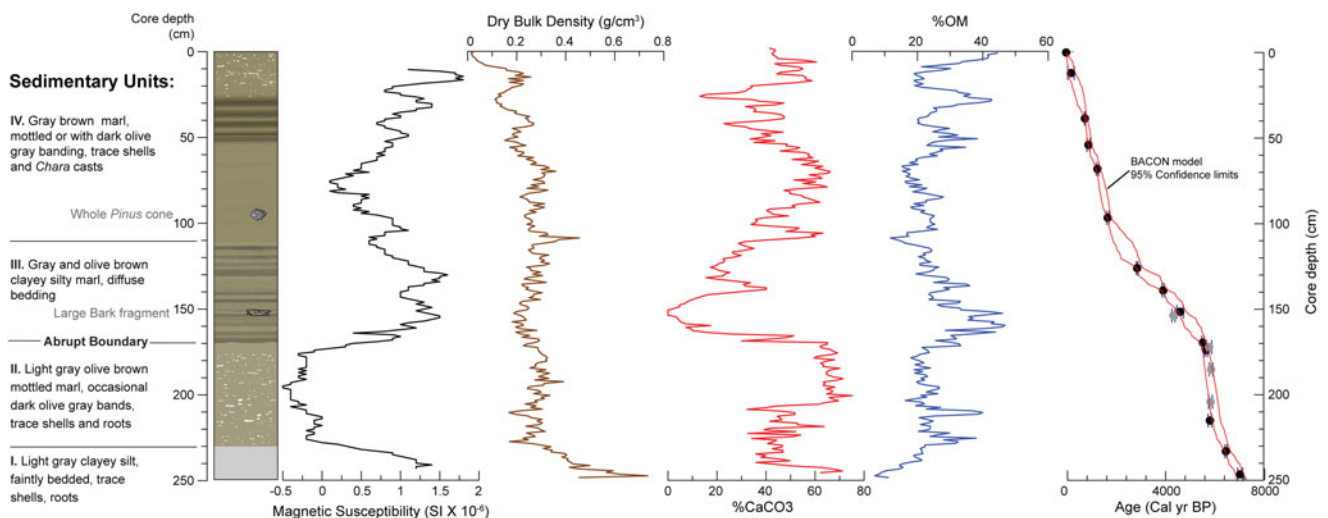


Figure 5. Core D lithologic units, bulk magnetic susceptibility (black) and dry bulk density (brown), percent inorganic carbon (%CaCO₃, red) and organic matter (%OM, blue), and the age-depth model. Age control points are shown in black with 1σ error bars. Omitted ages are shown in gray. Red outlines denote the 95% confidence limits of the age model.

Table 2. Aqueous and isotopic geochemistry of Emerald Lake, Utah.

Parameter	Result	
<i>Surface Water Field Measurements</i>		
Temperature (°C)	16.2	
pH	8.9	
Specific conductivity (µS/cm)	97	
Dissolved Oxygen (mg/L)	9.9	
<i>Dissolved Ions (mg/L)</i>		
Ca	21.1	
Mg	7.3	
Na	0.6	
K	0.27	
Alkalinity	75.2	
Cl	0.62	
SO ₄	2.3	
Sr	107	
<i>Carbon and Oxygen Isotopes (‰VPDB)</i>		
	$\delta^{18}\text{O}$	$\delta^{13}\text{C}$
Lake water (2006)	-12.1	na
Lake water (2007)	-11.1	na
Surface sediment	-11.50	1.87
Predicted equilibrium value ¹	-11.23	
Living Chara	-13.09	-2.56
Bedrock (Flagstaff Fm)	-5.70	-8.31

¹Following the equations of Epstein et al. (1953), Tarutani et al. (1969), Friedman and O'Neil (1977)

Daphnia egg cases, fine rootlets, and insect parts. Terrestrial macrofossils include charcoal, bark and cone fragments, and needles of *Picea* sp. and *Pseudotsuga menziesii*. Dry bulk density values (~0.2 g/cm³) and low magnetic susceptibility (<1 SI) reflect the higher OM (20–40%) and carbonate (40–75%). Although mottled, the marl is strongly bedded, with alternating bands of slightly lighter and darker olive brown color.

The transition to Unit III is an abrupt boundary marked by a change in grain size texture and composition to a massive monochromatic silty gyttja (170–110 cm depth). The boundary is marked by an abrupt rise in magnetic susceptibility and % OM and a carbonate decline from ~70–20%. Above the boundary, dry bulk density values and color banding remain unchanged while the bedding becomes diffuse. A very large wood/bark fragment at 152 cm depth occurs with peak values of magnetic susceptibility where carbonate is entirely absent. Above this depth, a gradual rise in carbonate is tracked by declines in magnetic susceptibility and %OM. Macrofossils in Unit III are significantly less abundant than in all other units and, where present, are dominated by undifferentiated aquatic herbaceous material (Fig. S1).

The transition to the base of Unit IV (110–0 cm depth) is a gradual return to mottled textures and higher percentages of carbonate (>40%), with a decline in magnetic susceptibility values. Unit IV has similar macrofossil types as Unit II, is rich in *Picea* sp. needles, and includes *Chara* sp. stem casts, but lacks oogonia

and *Daphnia*. A complete and intact conifer cone occurs at 97 cm depth.

For this study, the sediment characteristics of Core A/C were evaluated in further detail and divided into two limnic facies based on composite core photographs (Fig. S2). Basal Unit I (296–250 cm) is bedded silty olive brown marl, with intermittent mottling, and high yet variable values of dry bulk density (0.4–0.6 g/cm³), percent carbonate (2–40%), and %OM (20–40%). Near the upper boundary of Unit I are occasional mm-scale white bands below a transition to massive olive brown gyttja, which characterizes Unit II (240–0 cm). Moving upwards through Unit II, dry bulk density values gradually decline to values near 0.1 g/cm³ for the upper 50 cm of the core. Throughout Unit II, OM fluctuates between 25–40%, whereas percent carbonate is near zero at the base and gradually rises and remains near ~25% before a decline to near zero in the upper 30 cm.

Age Models and Sedimentation Rates

Age-depth models were generated using the Bayesian software 'rbacon' package v.2.5.3 in R (Blaauw and Christen, 2011; Blaauw et al., 2021), which includes IntCal20 calibrations. Default prior assumptions were used. For core D, three aquatic plant macrofossil samples at 173 cm, 186 cm, and 205 cm depth were omitted because the median calibrated reservoir-corrected ages were statistically identical to one another within the range of 1σ error. The large bark fragment sample at 154 cm depth was omitted because the age of 4295 cal yr BP was stratigraphically young by several centuries, possibly because of settling due to its large size. The resulting model for Core D has an average error range of ± 170 years with a maximum of ± 330 years between 100–150 cm depth, where a single aquatic *Potamogeton* sp. seed at 126 cm was the only suitable material to be found. The average rate of sediment accumulation for core D is 0.06 ± 0.07 cm/yr. Maximum rates of 0.26 cm/yr occur within Unit II, between ca. 6000–5600 cal yr BP, below the abrupt boundary. Minimum rates of 0.012 cm/yr occur within Unit III between 4000–2800 cal yr BP.

For core A/C, one unusually old age at 81 cm depth of 2520 cal yr BP from a conifer needle was omitted because it generated unrealistic changes in sedimentation rates. The resulting error range for core A/C age is larger than core D, with an average of ± 300 years and maximum of ± 700 years where ages were extrapolated to the bottom of the core (Fig. S2). Core A/C sediment accumulation rates are 0.06 ± 0.06 cm/yr, with maximum rates of 0.25 cm/yr occurring within the upper 5 cm, which represents that past ca. 50 years. Minimum rates of 0.010 cm/yr occur at the base of the core from ca. 10,000–6500 cal yr BP.

Mineralogy

Core D mineral sediments are composed of calcite with lesser dolomite, quartz, and feldspar, which are detrital minerals in this setting (Figs. 6, S3). Prominent mineralogic change corresponds with the four lithic units that are hereafter described by age. Between 7150–5530 cal yr BP, in Units I and II, calcite is dominant (40–60%) with minor quartz (~10%), trace dolomite and feldspar (<3%). At ca. 5500 cal yr BP, an abrupt rise in dolomite (+25%) and quartz (+5%) occur with major decline in calcite (–60%) that coincides with the depth of the abrupt boundary that marks the transition from Unit II to III. During the next several centuries, calcite is absent as dolomite and quartz gradually

decline to trace values by ca. 5000 cal yr BP. By ca. 4700 cal yr BP trace amounts of calcite reappear intermittently before an abrupt rise in quartz (+30%) at ca. 4500 cal yr BP, which becomes the dominant mineral (up to 45%) between ca. 4500–2650 cal yr BP, with minor calcite (10–20%) and trace dolomite (~5%). Over the next two centuries (ca. 2650–2450 cal yr BP) quartz values decline precipitously to trace levels, with several rapid fluctuations of 20–30%, as calcite increases by +40% to become the dominant mineral (>50%) in Unit I. Within Unit I, lower calcite abundances occurred during brief peaks in quartz (~30%) at ca. 1000 cal yr BP and 500 cal yr BP.

Carbonate Stable Isotopes

Core D isotope results of bulk carbonate analyses reflect varying proportions of endogenic calcite, detrital dolomite, and detrital calcite. A binary endogenic calcite and detrital dolomite mixture is assessed by taking the fraction of dolomite (of total carbonate) multiplied by Flagstaff dolomite values of -5.7‰ for $\delta^{18}\text{O}$ and -8.3‰ for $\delta^{13}\text{C}$ (Bowen et al., 2008), subtracted from raw $\delta^{18}\text{O}$ and $\delta^{13}\text{C}$ values, respectively, and divided by the fraction of calcite of total carbonate.

$$\delta^{18}\text{O}_{\text{Norm}} = [\delta^{18}\text{O}_{\text{raw}} - f_{\text{dolomite}} \times -5.7] / f_{\text{calcite}}$$

and

$$\delta^{13}\text{C}_{\text{Norm}} = [\delta^{13}\text{C}_{\text{raw}} - f_{\text{dolomite}} \times -8.3] / f_{\text{calcite}}$$

The result of dolomite normalization lowers raw carbonate isotope values up to -2‰ for oxygen and carbon, in proportion to dolomite abundance (Fig. S4). Normalized $\delta^{18}\text{O}$ values range from approximately -9‰ to -16‰ , which overlap values of

modern sediments and living *Chara*. Normalized $\delta^{13}\text{C}$ values range from $\sim 2\text{‰}$ to -2‰ , and the structure of the raw stratigraphic isotopic trends for both C and O remains intact. Between ca. 7150–6750 cal yr BP, dolomite-normalized values of $\delta^{18}\text{O}$ (Unit I) vary between -14‰ and -16‰ (Fig. 6). From 6750–5530 cal yr BP (Unit II) values increase, varying between -13.5‰ and -12.5‰ . The loss of carbonate at the time of the abrupt boundary, ca. 5500 cal yr BP, interrupts the isotope record, therefore no data could be obtained (Unit III). The $\delta^{18}\text{O}$ record resumes at ca. 4000 cal yr BP (Unit IV) with an increase in values to -10‰ at ca. 3500 cal yr BP, which coincides with high proportions of detrital quartz. At ca. 2500 cal yr BP, values precipitously decline to -14.5‰ in <500 years, with a corresponding decline in detrital quartz. Subsequently, when detrital minerals are at trace levels, $\delta^{18}\text{O}$ values abruptly rise to approximately -12‰ by ca. 2000 cal yr BP and decline to approximately -14.5‰ by ca. 1600 cal yr BP. For the past ca. 1500 years, values vary between -14‰ and -13‰ . The exceptions are two prominent positive excursions to values near -10‰ , which coincided with a rise in detrital quartz at ca. 1000 cal yr BP and 500 cal yr BP.

Dolomite-normalized values of $\delta^{13}\text{C}$ covary with higher $\delta^{18}\text{O}$ values that are greater than -12‰ in a manner that is commonly observed for hydrologically closed lakes (Talbot, 1990; Horton et al., 2016), which also coincides with higher proportions of detrital minerals (Fig. 7). Low δ values in both isotopes are more widely scattered, which is frequently observed for lakes with shorter residence times and higher hydrologic connectivity through sub-surface flow. Higher carbonate abundance in Emerald Lake occurs with lower lake $\delta^{18}\text{O}$ values, a relationship that previously has been observed to indicate that reductions in calcium-rich groundwater inflow in response to dry conditions also can impose limitations on carbonate production (Shapley et al., 2005).

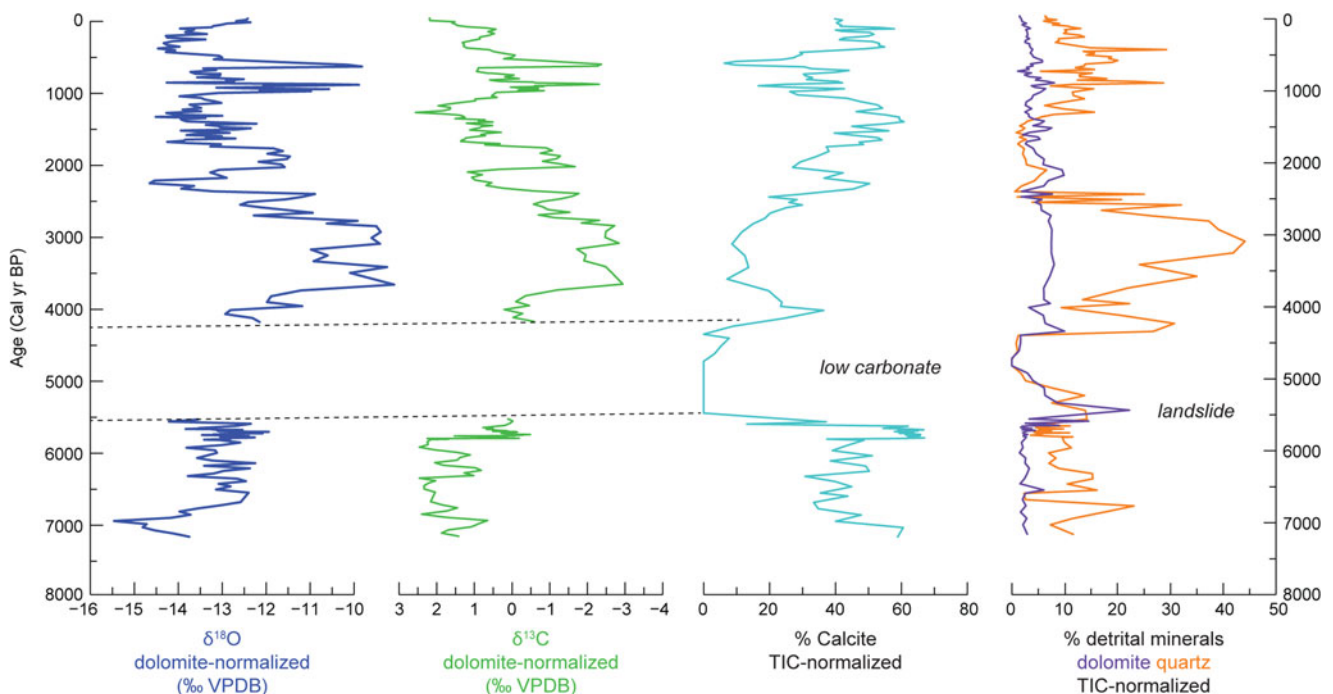


Figure 6. Core D carbonate $\delta^{18}\text{O}$ and $\delta^{13}\text{C}$ (dolomite-normalized, note reversed $\delta^{13}\text{C}$ axis) shown with abundances of calcite, dolomite (purple), and quartz (orange) plotted against age (cal yr BP). Percentages of dolomite indicate detrital influence on calcite abundance and are used to normalize the carbonate isotope values. Mineral abundances are normalized by percent carbonate using coulometric values of Total Inorganic Carbon (TIC).

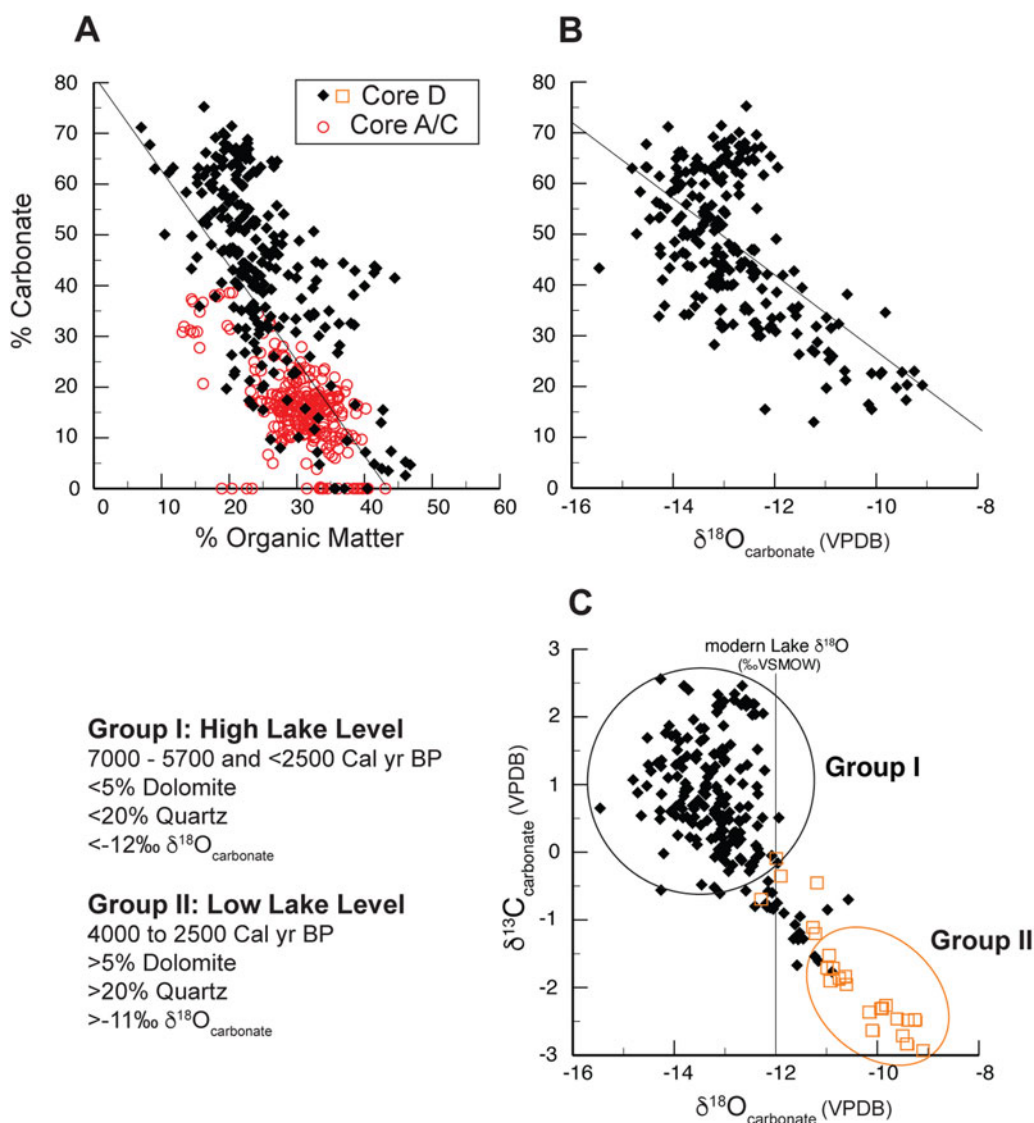


Figure 7. Sediment associations for (A) organic matter and carbonate abundances, core D in solid black, core A/C in open red. (B) Core D percent carbonate and carbonate $\delta^{18}\text{O}$ (dolomite normalized), and (C) carbonate $\delta^{18}\text{O}$ and $\delta^{13}\text{C}$ (dolomite normalized) grouped by detrital mineral abundance (higher in open orange) and inferred lake level.

DISCUSSION

The results from Emerald Lake are discussed first in terms of lake-level change, including the landslide event, based on the interpretation of sedimentology, mineralogy, and geochronology from both sediment cores A/C and D (Figs. 8, 9). This is followed by the rationale for the carbonate oxygen isotope interpretation of core D and the paleoclimatic reconstruction for the high plateau region of central Utah (Fig. 10). The reconstruction is then compared with regional records in the Upper Colorado River basin, the Great Basin, and the northern Rocky Mountain regions, including comments regarding the 'Late Holocene Dry Period' (Mensing et al., 2013).

Holocene lake levels and landslide activity

Following the last retreat of Pleistocene glaciers on the Wasatch Plateau, early Holocene limnic sedimentation began in the Emerald Lake basin by at least ca. 10,000 cal yr BP, according to an age from core A/C that is ~40 cm above the base of

lacustrine sediments. The onset could be as early as ca. 11,300 cal yr BP, if age model extrapolation to the base of the core is accurate (Fig. S2). Relatively dry Early Holocene conditions are indicated by slow sedimentation rates, whereas high carbonate preservation in core A/C suggests that the early lake was too shallow to support extensive carbonate dissolution, either endogenic or allocthonous, within the water column (e.g., <4 m depth; Fig. 4A). Significant organic matter accumulation indicates that the early shallow pond was biologically productive. This is consistent with pollen indicators, including cattail (*Typha* spp.) and willow (*Salix* spp.), within a sub-alpine spruce-fir forest. Relatively low charcoal levels indicate an infrequent and relatively low-severity fire regime (Morris et al., 2015).

After ca. 8500 cal yr BP, increased carbonate in core A/C and corresponding organic matter decline is consistent with processes whereby organic carbon production promotes or deters carbonate preservation by regulating rates of dissolution, commonly known as the 'carbon pump' (Dean, 1999; Wittkop et al., 2009; Fig. 7A). However, rising carbonate amounts also could indicate reworking

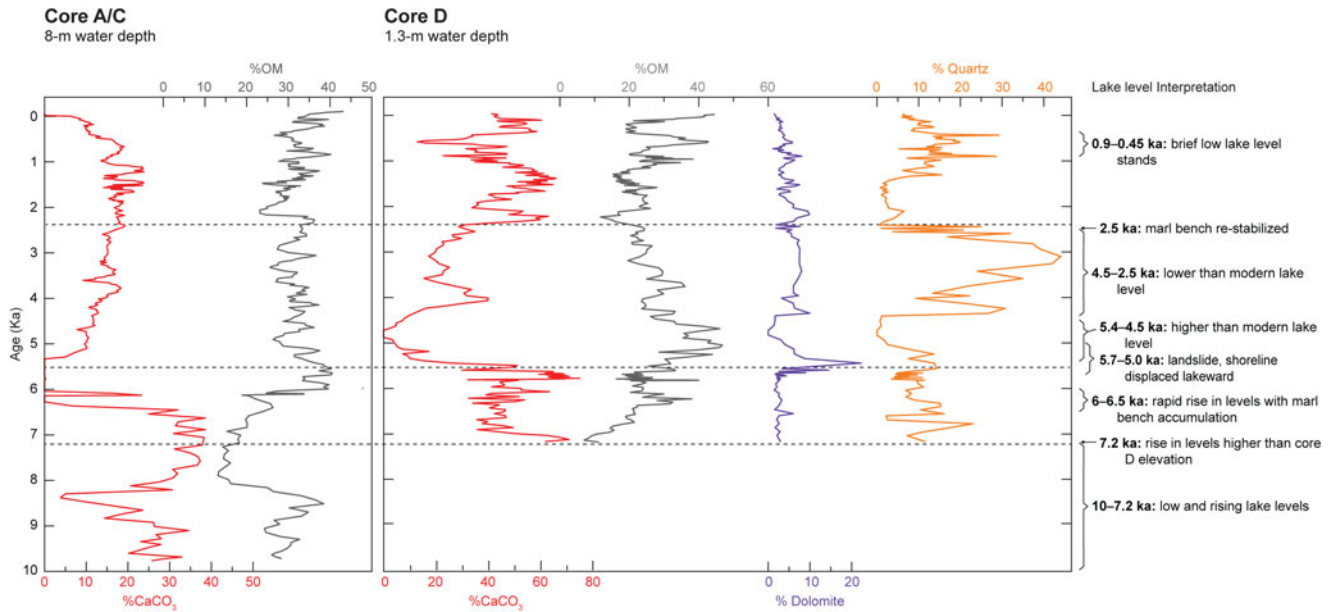


Figure 8. Stratigraphic variations in sediment composition for core A/C (left, 8 m water depth) and core D (middle, 1.3 m water depth) with chronological lake level interpretations (right). All units are in percent for carbonate (red, CaCO_3), organic matter (black, OM), and, for core D, detrital dolomite (purple), and quartz (orange).

of material from early development of the marl bench around the margins of the lake's depocenter (Figs. 3B, 9).

By ca. 7200 cal yr BP, marl accumulation began at the core D location while carbonate abundance in deeper water depths remained unaltered, indicating that lake levels had risen to water depths of ~5–5.5 m, thereby allowing sediment accumulation at

the core D site. Subsequent rapid accumulation of shallow water marl in core D (by ~50 cm) between ca. 6500–5500 cal yr BP indicates rising lake levels to depths exceeding ~6.5–7 m. The corresponding carbonate decline in core A/C also supports a deeper water column, enhanced stratification, and higher carbonate dissolution in the hypolimnion. This Early to Middle Holocene lake

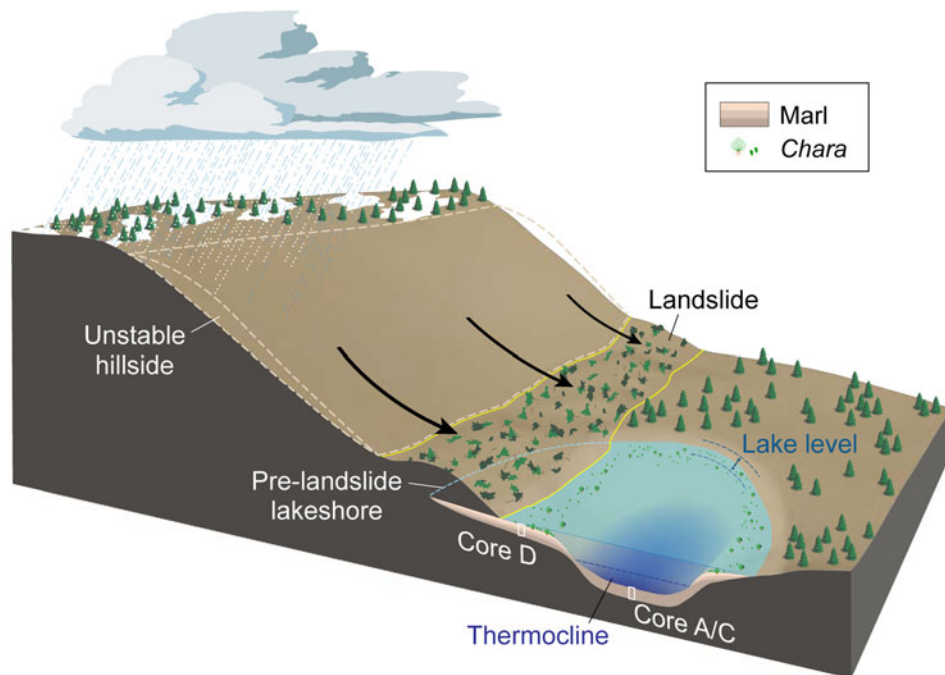


Figure 9. Schematic illustration of the Emerald Lake basin across A-A' (Fig. 3C) showing the lake and watershed processes affected by the landslide at the core A/C and D locations. During a wet period with rising lake levels (ca. 5500 cal yr BP), a landslide moved down the unstable cirque hillslope and entered the lake, moving towards the core D location and reducing the lake's volume. Stratification of the lake's water column led to higher sedimentary carbonate abundances above the thermocline, producing marl benches (light blue water color) rich in *Chara* (green algae). Less carbonate accumulated below the thermocline (dark blue) because carbonate dissolved while settling through the water column. Lake stratification strengthened with higher lake levels and weakened with lower lake levels.

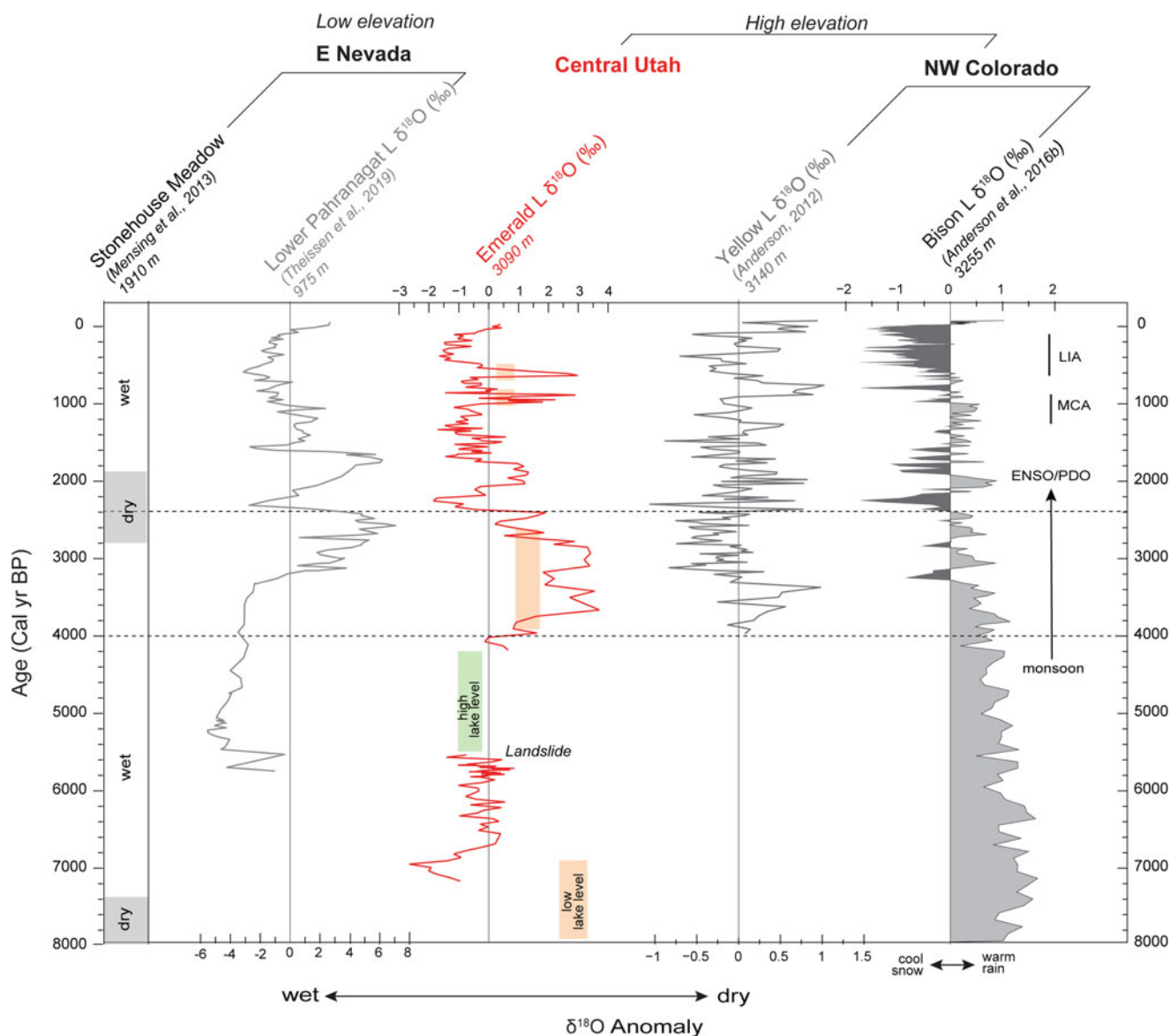


Figure 10. Regional record comparison between latitude 37° and 40°N from low-elevation western sites (left, 114.5°W, eastern Nevada) to high-elevation eastern sites (right, 107°W, western Colorado). Inferred wet and dry periods at Stonehouse Meadow (1910 m elevation; Mensing et al., 2013); $\delta^{18}\text{O}$ anomalies at Lower Pahranaagat Lake (975 m elevation; Theissen et al., 2019). Emerald Lake (red, this study) in central Utah (3090 m elevation) with periods of low lake levels indicated by orange shaded boxes to the right of the vertical Holocene average and high lake levels in green to the left, and Yellow and Bison lakes (3140 m and 3255 m elevation, respectively; Anderson, 2011, 2012; Anderson et al., 2016a, 2016b), which indicate a precipitation transition from summer monsoon to winter ENSO/PDO regimes. LIA = Little Ice Age, MCA = Medieval Climate Anomaly.

level rise indicates increasingly wet conditions coinciding with a period of limited fire conditions (Morris et al., 2015) before landslide movement down the cirque face into Emerald Lake occurred.

The landslide is documented by core D sediments, proximal to the slump toe (Fig. 9) by (1) a prominent sedimentary change; (2) disappearance of endogenic carbonate; and (3) a pulse in detrital minerals, all at a stratigraphic position that immediately overlies a radiocarbon age of ca. 5520 ± 50 cal yr BP. Therefore, the lake's sediment record is consistent with the slump toe superimposed onto the marl bench, which also indicates that the landslide post-dates marl bench development. Additionally, carbonate increased in the lake's depocenter (seen in core A/C), which is consistent with remobilization of shallow marl sediments. The lack of carbonate in core D between ca. 5400–4500 cal yr BP reflects raised

lake levels in response to the landslide, which disturbed near-shore sediments and inhibited marl bench growth, while the spike in detrital dolomite and quartz reflects the sudden change in available near-shore sediment.

After the landslide episode, a prominent rise in quartz at the core D location, beginning at ca. 4500 cal yr BP, is distinct from the inferred landslide detrital signature (Fig. 6). Although the initial increase in quartz is similar with a pulse in dolomite, the dolomite rise is smaller and then declines to trace levels as quartz continues to rise and remain elevated for the subsequent ca. 2000 years. In further contrast to the sediment record immediately after the landslide when endogenic carbonate disappears, here, endogenic carbonate begins to increase gradually. The interpretation of the quartz pulse is that it represents lake level

lowering and re-working of the shoreline sediments, perhaps in conjunction with erosion of the slump surface and dust inputs. Further investigation into the source of quartz, including soil development on the slump surface, is warranted.

The inferred lake level decline during this period coincides with an increase in charcoal abundance, reflecting increased fire frequency and severity (Morris et al., 2015). The lake's deep-water sediments were unaffected by lake level decline, likely because it was not great enough to alter either lake stratification or rates of carbonate dissolution. The increase in shallow water detrital quartz corresponds with inhibited marl bench growth indicated by reduced sedimentation rates. *Chara* thrives in undisturbed clear water in calm offshore areas, conditions that appear to return by ca. 2500 cal yr BP corresponding with quartz declines and rising water levels to modern conditions. During the past ca. 2500 years, near-modern lake levels indicate relatively wet conditions compared to the Middle and Early Holocene, although brief low stands and dry periods are indicated by higher frequency variations in quartz.

Oxygen isotope interpretation and paleoclimatic reconstruction

The stratigraphic variations in sedimentary carbonate $\delta^{18}\text{O}$ values (dolomite-normalized) are interpreted as a proxy for variations in lake $\delta^{18}\text{O}$ values based on modern data (Fig. 4B; Table 2), which indicate that carbonate sediments of endogenic origin are in isotopic equilibrium with lake water. In turn, Emerald Lake $\delta^{18}\text{O}$ is influenced by evaporative enrichment and shifts in the relative proportions of winter and summer precipitation, which strongly covary with precipitation source and temperature. Higher lake $\delta^{18}\text{O}$ values indicate increased rates of evaporation, relative to precipitation, during the ice-free season from June through September, and therefore lower effective moisture (i.e., lower P-E). Higher values may also reflect more summer rainfall relative to winter snowfall. Summer rainfall in the Upper Colorado River region is associated with warmer temperatures and convection of recycled moisture derived from the south (Friedman 2002a; Anderson 2012). Lower lake $\delta^{18}\text{O}$ values can reflect more winter snowfall relative to rainfall and higher effective moisture (i.e., higher P-E) if winter precipitation exceeds summer evaporation. In central Utah, winter snowfall is associated with cold temperatures and North Pacific moisture sources (Friedman, 2002a).

The resulting Emerald Lake $\delta^{18}\text{O}$ inferred paleoclimatic interpretation is described in terms of anomaly values relative to the Holocene average of -12.8‰ (Fig. 10), which is similar to the water isotope values of the modern lake. This approach standardizes the influence that detrital proportions of carbonate exert on absolute $\delta^{18}\text{O}$ values and differences. The interpretation of the lake's volumetric and isotopic evolution is carefully framed by the lake level reconstruction, which reflects changes in effective moisture and P-E.

Negative lake $\delta^{18}\text{O}$ anomalies from ca. 7200–6800 cal yr BP (Fig. 10) are attributed to higher effective moisture as lake levels rose and the lake's surface area expanded over the core D location. The early negative lake $\delta^{18}\text{O}$ anomalies could also reflect a local influence on nearshore carbonates by nearby spring discharge points, which can produce relatively low $\delta^{18}\text{O}$ values in the near vicinity. A lake-wide response to higher snowfall proportions is a less likely explanation considering the context of regional comparisons discussed in further detail below. Lake $\delta^{18}\text{O}$ anomalies were positive by ca. 6600 cal yr BP, and are interpreted to reflect a rain-dominated precipitation balance when lake levels rose in response

to higher effective moisture. Lake $\delta^{18}\text{O}$ anomalies subsequently fluctuated near the Holocene average as lake levels were rising in concert with marl bench sedimentation, suggesting lake-water isotopes were in steady state during increasingly wet climate conditions. The landslide occurrence at ca. 5500 cal yr BP during relatively wet paleohydrologic conditions potentially implicates a climatic trigger for the slope failure (e.g., Shurtliff et al., 2017). The lack of erosion in the lake sediment record, or presence of larger grained clasts, suggests low energy landslide movement such as slump-creep rather than movement in a rapid, catastrophic sense. However, there is currently no evidence that allows rejection of a seismic trigger related to any of the numerous faults within the area (Machette et al., 1991).

Between ca. 4000–2500 cal yr BP, positive $\delta^{18}\text{O}$ anomalies reflect low lake levels driven by dry climatic conditions (Fig. 10). The interval is exceptional in duration and demonstrates levels of aridity that approach the unprecedented aridity of the Early Holocene. By ca. 2800 cal yr BP, a return to wet conditions driven by higher amounts of snowfall relative to rainfall was underway, reflected by a shift to negative lake $\delta^{18}\text{O}$ anomalies between ca. 2200–2000 cal yr BP. A rapid shift from negative to positive anomalies between ca. 2000–1800 cal yr BP indicates a return to dry conditions that was relatively brief by comparison with previous dry periods. Subsequently, a wetter, cooler, snow-dominated climatology persisted between ca. 1800–1000 cal yr BP with negative lake $\delta^{18}\text{O}$ anomalies in an apparent isotopic steady state with wetter and colder climatic conditions. Hydroclimatic variations became more frequent during the Medieval Climate Anomaly (MCA; ca. 1000–700 cal yr BP, AD ca. 950–1250) with dry periods leading to low lake levels at ca. 1000 cal yr BP and 500 cal yr BP, potentially caused by reductions in winter precipitation and limited summer rains. In contrast, persistently negative lake $\delta^{18}\text{O}$ anomalies indicate a wet, cool, snow-dominated climatology during the Little Ice Age (LIA; ca. 650–100 cal yr BP, AD ca. 1300–1850). By comparison to the LIA, relatively reduced snowfall and dry conditions characterize the past ca. 100 years, which approximate the Holocene average.

Regional Comparison

The high elevation paleoclimatic reconstruction from Emerald Lake in central Utah based on multiproxy data shows paleoclimatic variations at time scales ranging from millennia to decades and allows for geographical comparison between the Great Basin of eastern Nevada and the Upper Colorado River basin (Fig. 10). Conditions that were significantly drier than modern occurred between ca. 10,000–7000 cal yr BP, as indicated by low and rising Emerald Lake levels. This result corresponds with orbital forcing by trends in summer solar insolation that are consistent with strengthened monsoon rainfall and concurrent with northward retreat of the Laurentide Ice sheet (Epstein and Xu, 1999; Sjoström et al., 2004; Anderson, 2011; Metcalf et al., 2015; Bhattacharya et al., 2018; Huth et al., 2020). During this period, isotopes of laminated soil carbonate rinds in Torrey, Utah, indicate a trend of low and rising soil moisture at low elevations (~1080 m elevation; Huth et al., 2020). Additionally, a dry early Holocene undergoing a rise in local moisture is inferred at Garden Basin Fen (2400 m elevation), on the slope of the Fish Lake Plateau, from pollen and diatom assemblages, which also corresponds with timing of the Windy Ridge landslide (Shurtliff et al., 2017). Although sub-regional climatic variations are

inherently intricate, the collective evidence supports that Early Holocene conditions were the driest of the epoch at latitude $\sim 39\text{--}40^\circ$ N, across the Upper Colorado River basin, from central Utah at Emerald Lake to northwest Colorado, which included contributions from southerly moisture sources usually associated with the monsoon and significant reductions in snowpack.

The rise to near-modern Emerald Lake levels by ca. 7500 cal yr BP and continued rise through at least ca. 5500 cal yr BP, with $\delta^{18}\text{O}$ variations near both modern and Holocene averages, is indisputable evidence for higher moisture compared to the Early Holocene. Additional evidence for wetter conditions during this period at low elevations in eastern Nevada (Fig. 10) includes initiation of the Spring Valley Stonehouse sedge-meadow (1910 m elevation) by ca. 7500 cal yr BP (Mensing et al., 2013), return of marshes at the Blue Lake wetland by ca. 6500 cal yr BP (Louderback and Rhode, 2009), and early lake development in the Pahranaagat Valley (975 m elevation) by ca. 5800 cal yr BP (Theissen et al., 2019). To the east in Colorado, rising effective moisture during this period is evident by a gradual decline in Bison Lake $\delta^{18}\text{O}$ values and overflowing lake levels at Yellow Lake (3090 m elevation; Anderson, 2012), as well as higher lake levels in the central Colorado Rockies at 3050 m elevation between 5700–4800 cal yr BP (Shuman et al., 2014). Although the landslide into Emerald Lake at ca. 5500 cal yr BP was a direct cause for an abrupt rise in lake level, higher levels may have stabilized subsequently between ca. 5500–4000 cal yr BP in part due to wetter conditions, although this is not certain.

These results contrast with interpretations by Lachniet et al. (2020) for aridity intervals at Leviathan Cave between ca. 9000–5000 cal yr BP based on elevated $\delta^{18}\text{O}$, $\delta^{13}\text{C}$, and slow speleothem growth rates. The elevated cave water $\delta^{18}\text{O}$ values in their study are also attributed to warmer temperatures; however, alternatives to their explanations also could include southerly moisture sources usually associated with the monsoon (e.g., Huth et al., 2020). The Leviathan $\delta^{18}\text{O}$ record shows a millennial scale decline between ca. 8000 and 5000 cal yr BP, which to some extent reflects a regional rise in effective moisture as recorded in the Emerald Lake record. Nevada speleothem $\delta^{18}\text{O}$, $\delta^{13}\text{C}$, and trace element records have shown contrasting trends in different caves (Lachniet et al., 2014; Steponaitis et al., 2015); differences in cave hydrology and/or disequilibrium with elevation are known to influence speleothem proxy sensitivity in unique ways (e.g., Johnston et al., 2013; Weber et al., 2021). In addition to cave drip water studies focused on relationships with meteoric water (Oster and Kelley, 2016), further investigations into surface water relationships are needed because they are directly incorporated into stalagmite proxies (e.g., Anderson et al., 2016b).

Following the Emerald Lake landslide at ca. 5500 cal yr BP, and the relatively wet period thereafter, a multi-millennial dry period between ca. 4000–2400 cal yr BP occurred, which envelopes a previously identified “Late Holocene Dry Period” (Mensing et al., 2013), potentially extending the spatial and temporal extent of this episode. The timing of higher Emerald Lake $\delta^{18}\text{O}$ anomalies and increased detrital minerals between ca. 4000–3500 cal yr BP corresponds with higher lake $\delta^{18}\text{O}$ values in the Yellow Lake record, which also suggest dry conditions (Fig. 6). Thereafter, the record comparison suggests a time-transgressive drought expansion, based on higher lake $\delta^{18}\text{O}$ values at Lower Pahranaagat Lake that occurred several centuries later, which was then followed by a rise in carbonate preservation at Stonehouse Meadow (attributed to dry conditions) that occurred another several centuries later.

The temporal differences of these shifts may approach the chronological uncertainties of the independent age models (e.g., Zimmerman and Wahl, 2020), leaving the possibility that some or all of the shifts either were nearly simultaneous, or that the progression of the pattern was slower or faster within centuries. However, it is interesting to note that within this dry interval a brief decline in $\delta^{18}\text{O}$ anomalies at Emerald and Yellow lakes at ca. 3,200 cal yr BP coincides with the earliest negative $\delta^{18}\text{O}$ anomaly of the Bison Lake record interpreted to reflect an increase in snow (relative to rain). Whereas the onset of the dry interval is interpreted to reflect lower precipitation and higher evaporation in response to a decline in monsoon precipitation that preceded an increase in snow, the negative $\delta^{18}\text{O}$ anomaly within the dry period appears to indicate the earliest sign of this transition. This result shows that the unprecedented nature of the mid-Holocene dry period reflects the unique seasonal insolation-driven transition from monsoon to snow, and that the latter half of the dry period was a fluctuating transition to the winter-dominated regime with periods of rapid climate change on time scales of multiple decades to centuries.

Although onset of the dry period appears transgressive, the return to wetter conditions at ca. 2400 cal yr BP was nearly synchronous with rapid shifts to negative $\delta^{18}\text{O}$ anomalies registered at Lower Pahranaagat, Emerald, Yellow, and Bison, indicating complete transition to higher snowfall (relative to rain) on a regional scale at high and low elevations. By ca. 2000 cal yr BP, a rapid return to dry conditions was simultaneously registered by positive lake $\delta^{18}\text{O}$ anomalies at all four of the sites, which persisted for multiple decades to centuries, and corresponds with multi-decadal drought recorded by tree-ring chronologies in northeastern Utah and the southern San Juan Mountains of Colorado (Knight et al., 2010; Routson et al., 2011). This early first millennium dry period is not so clearly registered in northwestern Colorado at Bison and Yellow lakes, which indicate high snowfall and effective moisture conditions near the Holocene average. If this difference represents a northeast-to-southwest precipitation pattern, it is consistent with persistent atmospheric ridging found currently over the Great Basin and jet stream flow over the northern Colorado Rockies driven by the influence of El Niño Southern Oscillation (ENSO) and Pacific Decadal Oscillation (PDO) regimes (Barron and Anderson, 2011; Steinman et al., 2014; Liu et al., 2014; Anderson et al., 2016b; Du et al., 2020, 2021).

By ca. 1700 cal yr BP, a rapid shift to higher snowfall (relative to rain) and effective moisture occurred at Emerald and Lower Pahranaagat lakes, and persisted at Emerald Lake over the next several centuries. A similar shift to persistent cool and wet conditions at this time is also observed in the northern Rockies (Stone et al., 2016; Larsen et al., 2020; Brown et al., 2021). An elevation contrast is suggested at Lower Pahranaagat, which returned to slightly dry or average effective moisture, and a west-east difference across the UCB is suggested by dry conditions at Bison and Yellow lakes. These geographic differences may reflect precipitation patterns with spatial dipole characteristics similar in complexity to those identified by more distant precipitation $\delta^{18}\text{O}$ and effective moisture comparisons along the margin of western North America from Alaska to southern California (Barron and Anderson, 2011; Steinman et al., 2014; Anderson et al., 2016a).

The MCA (ca. 1000–700 cal yr BP, AD ca. 800–1300) is characterized by prominent shifts to dry conditions at Emerald Lake at ca. 1000 cal yr BP and at ca. 500 cal yr BP, which is consistent with tree-ring chronologies in northeastern Utah that indicate prolonged droughts by ca. 800 cal yr BP and unprecedented drought at ca. 500 cal yr BP (Knight et al., 2010). Large variations

in snowpack occurred at this time in northwest Colorado at Bison and Yellow lakes, including dry periods, whereas there is no evident trend at low elevation Great Basin records (Lund and Benson, 2018; Munroe et al., 2018). At this geographic scale, spatial precipitation patterns likely reflect synoptic-scale climatology that support observations by Metcalf et al. (2015) who found considerable variability in the monsoon region during the MCA, which may reflect transient upper level ridging (Hermann et al., 2018) and/or persistent El Niño or La Niña regimes that affected both snowpack and summer rains (Anderson, 2012; Hart et al., 2021). The ubiquitously cold and wet LIA pattern observed at all high-elevation lakes in the UCB is also associated with wet conditions at low elevations (Lower Pahrangat Lake, Stonehouse Meadow) and indicates that high winter snowfall driven by jet stream positioning over the intermountain west region persisted for multiple decades.

CONCLUSIONS

Paleoclimate histories that include surface hydrologic response across elevation gradients provide a means to understand natural variations in water supply, and thereby better inform water management for the intermountain west. The new Emerald Lake record combined with other records at ~40°N indicate that throughout the Holocene, extreme dry periods with significant reductions in high elevation snowpack have occurred from the Great Basin to the Upper Colorado headwaters. With the growing collection of high-elevation isotope records, we can begin to place recent changes in snowpack in sub-regions of the UCB, and corresponding water supply variations, within a framework of millennial timescales. The Holocene extremes in snowpack variations expand upon observations based on shorter intervals (Pederson et al., 2011; Routson et al., 2011). The Emerald Lake record shows that the Upper Colorado River basin snowpack has undergone high magnitude change on a range of timescales, and that similar variations should be assessed within a twenty-first century context with caution. Framing observed trends within a longer context of multiple centuries to millennia allows more confident identification of significant trends, which will be essential to recognize in terms of future effects on regional water supplies.

Consideration of the evidence herein with respect to the introductory questions is pertinent to the future prognosis for intermountain snowpack. To address the first research question, if Holocene paleohydrologic trends were consistent at high and low elevations, the proxy results show that consistent paleohydrologic variations at both high and low elevations and on millennial to multi-century timescales are common. Consistent multi-decadal variations also appear to occur nearly simultaneously, particularly when snowfall variations during the past ca. 2500 years dominated paleohydrologic trends, although chronological precision at these timescales is currently insufficient for confident correlations. This finding validates regional representation of paleohydrologic reconstructions from low-elevation lakes and wetlands, and these records can be confidently used to represent water source variations. To address the second research question, if paleohydrologic extremes in the Upper Colorado were typically basin-wide or if sub-regional variations common, the results confirm that precipitation extremes in the Upper Colorado were commonly basin-wide, which implies synoptic scale climate-forcing mechanisms, and thereby a potential for predictability. However, varied sub-regional differences are also found, which addresses the third research question that regional precipitation

patterns with spatial dipole characteristics (e.g., wet north and dry south) and/or time-transgressive patterns have occurred that bear resemblance to historical patterns. A prominent example is within the expanded envelope of the 'Late Holocene Dry Period' proposed here. The Late Holocene Dry Period also provides one prominent example, of many, that addresses the fourth research question that numerous instances of non-analogue drought conditions are shown here to surpass those of the past 2000 years in severity and duration.

The Emerald Lake paleohydrologic record, located at the boundary of the three major sub-regions of the intermountain west—the Great Basin, Upper Colorado River basin, and the Colorado Plateau—brings clearer focus to the range of precipitation patterns and associated atmospheric transitions that can be anticipated to affect regional water supply in the future. There remain numerous western mountain ranges incorporating limestone substrates with small landslide-affected (or -formed) lakes in alpine settings that have yet to be fully investigated (e.g., Shapley et al., 2021). This study also provides a framework for future investigations of the paleoclimatic signals embedded in their lithology and carbonate isotope geochemistry.

Acknowledgments. The USGS ScienceBase data release for this publication can be located at <https://doi.org/10.5066/P9CZVFVNJ>. This research is supported by the U.S. Geological Survey Climate Research and Development Program. We thank Andrea Brunelle and Jesse Morris, who provided logistical support and field assistance that made this research possible. David Dettman at the University of Arizona and Million Hailemichael at Idaho State University provided carbonate and water isotope data; Core D AMS radiocarbon ages were provided by Jack Reed at the USGS Radiocarbon Laboratory and Chad Wolack at the Institute for Arctic Antarctic and Alpine Research (INSTAAR) at the University of Colorado Boulder. Alisa Mast at the USGS Colorado Water Science Center provided water chemistry data. We appreciate reviews by Marith Reheis and Paul Henne and two anonymous journal reviewers for their constructive suggestions that served to significantly improve the manuscript. Any use of trade, firm, or product names is for descriptive purposes only and does not imply endorsement by the U.S. Government.

Supplementary Material. The Supplementary Material for this article can be found at <https://doi.org/10.1017/qua.2022.42>.

REFERENCES

- Adams, D.K., Comrie, A.C., 1997. The North American Monsoon. *Bulletin of the American Meteorological Society* **78**, 2197–2213.
- Anderson, L., 2011. Holocene record of precipitation seasonality from lake calcite $\delta^{18}\text{O}$ in the central Rocky Mountains, United States. *Geology* **39**, 211–214.
- Anderson, L., 2012. Rocky Mountain hydroclimate: Holocene variability and the role of insolation, ENSO, and the North American monsoon. *Global and Planetary Change* **92–93**, 198–208.
- Anderson, L., Berkelhammer, M., Barron, J.A., Steinman B.A., Finney, B.P., Abbott, M.B., 2016a. Lake oxygen isotopes as recorders of North American Rocky Mountain hydroclimate: Holocene patterns and variability at multi-decadal to millennial time scales. *Global and Planetary Change* **137**, 131–148.
- Anderson, L., Berkelhammer, M., Mast, M.A., 2016b. Isotopes in North American Rocky Mountain snowpack 1993–2014. *Quaternary Science Reviews* **131**, 262–273.
- Barron, J., Anderson, L., 2011. Enhanced Late Holocene ENSO/PDO expression along the margins of the eastern North Pacific. *Quaternary International* **235**, 3–12.
- Bartlein, P.J., Anderson, K.H., Anderson, P.M., Edwards, M.E., Mock, C.J., Thompson, R.S., Webb, R.S., Webb, T.I., Whitlock, C., 1998. Paleoclimate simulations for North America over the past 21,000 years:

- features of the simulated climate and comparisons with paleoenvironmental data. *Quaternary Science Reviews* **17**, 549–585.
- Baum, R.L., Fleming, R.W.**, 1989. Landslides and debris flows in Ephraim Canyon, central Utah. *U.S. Geological Survey Bulletin* **1842-C**, C1–C12.
- Benson, L., Kashgarian, M., Rye, R., Lund, S., Paillet, F., Smoot, J., Kester, C., Mensing, S., Meko, D., Lindström, S.**, 2002. Holocene multidecadal and multicentennial droughts affecting Northern California and Nevada. *Quaternary Science Reviews* **21**, 659–682.
- Bhattacharya, T., Tierney, J.E., Addison, J.A., Murray, J.W.**, 2018. Ice-sheet modulation of deglacial North American monsoon intensification. *Nature Geoscience* **11**, 848–852.
- Blaauw, M., Christen, J.A.**, 2011. Flexible paleoclimate age-depth models using an autoregressive gamma process. *Bayesian Analysis* **6**(3), 457–474
- Blaauw, M., Christen, J.A., Aquino Lopez, M.A., Vazquez, J.E., Gonzalez, J.E., Belding, T., Theiler, J., Gough, B., Karney, C.**, 2021. Package “rbacon”, accessed 2021-Aug-12. <https://cran.r-project.org/web/packages/rbacon/rbacon.pdf>.
- Bowen, G.J., Daniels, A.L., Bowen, B.B.**, 2008. Paleoenvironmental isotope geochemistry and paragenesis of lacustrine and palustrine carbonates, Flagstaff Formation, central Utah, U.S.A. *Journal of Sedimentary Research* **78**, 162–174.
- Bright, J., Kaufman, D.S., Forester, R.M., Dean, W.E.**, 2006. A continuous 250,000yr record of oxygen and carbon isotopes in ostracode and bulk-sediment carbonate from Bear Lake, Utah-Idaho. *Quaternary Science Reviews* **25**, 2258–2270.
- Brown, S.R., Cartier, R., Schiller, C.M., Zahajská, P., Fritz, S.C., Morgan, L.A., Whitlock, C., et al.**, 2021. Multi-proxy record of Holocene paleoenvironmental conditions from Yellowstone Lake, Wyoming, USA. *Quaternary Science Reviews* **274**, 107275. <https://doi.org/10.1016/j.quascirev.2021.107275>.
- Bryson, R.A., Hare, F.K.**, 1974. *Climates of North America*. World Survey of Climatology, Vol. 11. Elsevier Scientific Publishing Company, Amsterdam, London, New York, 420 pp.
- Dean, W.E.**, 1999. The carbon cycle and biogeochemical changes in lake sediments. *Journal of Paleolimnology* **21**, 375–393.
- Dean, W.E., Forester, R.M., Bright, J., Anderson, R.Y.**, 2007. Influence of the diversion of Bear River into Bear Lake (Utah and Idaho) on the environment of deposition of carbonate minerals. *Limnology and Oceanography* **52**, 1094–1111.
- DeGraff, J.V.**, 1978. Regional landslide evaluation: two Utah examples. *Environmental Geology* **2**, 203–214.
- Dohrenwend, J.C.**, 1984. Nivation landforms in the western Great Basin and their paleoclimatic significance. *Quaternary Research* **22**(3), 275–288.
- DuRoss, C.B., Personius, S.F., Crone, A.J., Olig, S.S., Hylland, M.D., Lund, W.R., Schwartz, D.P.**, 2016. Fault segmentation: new concepts from the Wasatch Fault Zone, Utah, USA. *Journal of Geophysical Research: Solid Earth* **121**, 1131–1157.
- Du, X., Hendy, I., Hinnov, L., Brown, E., Schimmelmann, A., Pak, D.**, 2020. Interannual southern California precipitation variability during the common era and the ENSO teleconnection. *Geophysical Research Letters* **47**, e2019GL085891. <https://doi.org/10.1029/2019GL085891>.
- Du, X., Hendy, I., Hinnov, L., Brown, E., Zhu, J., Poulsen, C.J.**, 2021. High-resolution interannual precipitation reconstruction of southern California: implications for Holocene ENSO evolution. *Earth and Planetary Science Letters* **554**, 116670. <https://doi.org/10.1016/j.epsl.2020.116670>.
- Dymerski A.D., Anhold J.A., Munson A.S.**, 2001. Spruce beetle (*Dendroctonus rufipennis*) outbreak in engelmann spruce (*Picea engelmannii*) in central Utah, 1986–1998. *Western North American Naturalist* **61**, 19–24.
- Engleman, E.E., Jackson, L.L., Norton, D.R.**, 1985. Determination of carbonate carbon in geological materials by coulometric titration. *Chemical Geology* **53**, 125–128.
- Epstein, S., Buchsbaum, R., Lowestam, H.A., Urey, H.C.**, 1953. Revised carbonate-water temperature scale. *Geological Society of America Bulletin* **62**, 417–426.
- Epstein, S., Xu, X.**, 1999. A climatic record from ¹⁴C-dated wood fragments from southwestern Colorado. *Global Biogeochemical Cycles* **13**, 781–784.
- Fleming, R.W., Johnson, R.B., Schuster, R.L.**, 1988. The Manti, Utah, landslide. *US Geological Survey Professional Paper* **1311**, 1–22.
- Friedman, I.**, 2002a. Stable isotope composition of waters in the Great Basin, United States 1. Air-mass trajectories. *Journal of Geophysical Research* **107** (D19), 4400. <https://doi.org/10.1029/2001JD000565>.
- Friedman, I.**, 2002b. Stable isotope compositions of waters in the Great Basin, United States 2. Modern precipitation. *Journal of Geophysical Research* **107** (D19), 4401. <https://doi.org/10.1029/2001JD000566>.
- Friedman, I., O’Neil, J.R.**, 1977. Compilation of stable isotope fractionation factors of geochemical interest. *U.S. Geological Survey Professional Paper* 440-KK, 11pp.
- Gibson, J.J., Birks, S.J., Yi, Y.**, 2016. Stable isotope mass balance of lakes: a contemporary perspective. *Quaternary Science Reviews* **131**, 316–328.
- Gibson, J.J., Edwards, T.W.D., Prowse, T.D.**, 1996. Development and validation of an isotopic method for estimating lake evaporation. *Hydrological processes* **10**, 1369–1382.
- Gillette, D.D., Madsen, D.B.**, 1992. The short-faced bear *Arctodus simus* from the late Quaternary in the Wasatch Mountains of central Utah. *Journal of Vertebrate Paleontology* **12**, 107–112.
- Gillette D.D., Madsen D.B.**, 1993. The columbian mammoth, *Mammuthus columbi*, from the Wasatch Mountains of central Utah. *Journal of Paleontology* **67**, 669–680.
- Glew, J.R., Smol, J.P., Last, W.M.**, 2001. Sediment core collection and extrusion. In: Last, W., Smol, J.P. (Eds.). *Tracking Environmental Change Using Lake Sediments: Basin Coring, and Chronological Techniques, Vol. 1*. Kluwer Academic Press, Dordrecht, Netherlands, pp. 77–105.
- Hart, I.A., Brenner-Coltrain, J., Boomgard, S., Brunelle, A., Coats, L., Metcalfe, D., Lewis, M.**, 2021. Evidence for a winter-snowpack derived water source for the Fremont maize farmers of Range Creek Canyon, Utah, USA. *The Holocene* **31**, 446–456.
- Hermann, N.W., Oster, J.L., Ibarra, D.E.**, 2018. Spatial patterns and driving mechanisms of mid-Holocene hydroclimate in western North America. *Journal of Quaternary Science* **33**, 421–434.
- Higgins, R.W., Mo, K.C., Yao, Y.**, 1998. Interannual variability of the U.S. summer precipitation regime with emphasis on the southwestern monsoon. *Journal of Climate* **11**, 2582–2606.
- Horton, T.W., Defliese, W.F., Tripathi, A.K., Oze, C.**, 2016. Evaporation induced ¹⁸O and ¹³C enrichment in lake systems: a global perspective on hydrologic balance effects. *Quaternary Science Reviews* **131**, 365–379.
- Huth, T.E., Cerling, T.E., Marchetti, D.W., Bowling, D.R., Ellwein, A.L., Passey, B.H., Fernandez, D.P., Valley, J.W., Orland, I.J.**, 2020. Laminated soil carbonate rinds as a paleoclimate archive of the Colorado Plateau. *Geochimica et Cosmochimica Acta* **282**, 227–244.
- Johnston V.E., Borsato A., Spötl C., Frisia S., Miorandi R.**, 2013. Stable isotopes in caves over altitudinal gradients: fractionation behaviour and inferences for speleothem sensitivity to climate change. *Climate of the Past* **9**, 99–118.
- Knight, T.A., Meko, D.M., Baisan, C.H.**, 2010. A bimillennial-length tree-ring reconstruction of precipitation for the Tavaputs Plateau, northeastern Utah. *Quaternary Research* **73**, 107–117.
- Lachniet, M.S., Asmerom, Y., Polyak, V., Denniston, R.**, 2020. Great Basin paleoclimate and aridity linked to Arctic warming and tropical Pacific sea surface temperatures. *Paleoceanography and Paleoclimatology* **35**, e2019PA003785. <https://doi.org/10.1029/2019PA003785>.
- Lachniet, M.S., Dennison, R.F., Asmerom, Y., Polyak, V.**, 2014. Orbital control of western North America atmospheric circulation and climate over two glacial cycles. *Nature Communications* **5**, 3805. <https://doi.org/10.1038/ncomms4805>.
- Larsen, D.J., Crump, S.E., Blumm, A.**, 2020. Alpine glacier resilience and Neoglacial fluctuations linked to Holocene snowfall trends in the western United States. *Science Advances* **6**, eabc7661. <https://doi.org/10.1126/sciadv.abc7661>.
- Larson, P.R.**, 1996. *Glacial Geomorphology of a Portion of the Wasatch Plateau, Central Utah*. Ph.D. Dissertation, Department of Geography, University of Utah, Salt Lake City, UT.
- Li, H.-C., Ku, T.-L., Stott, L.D., Anderson, R.F.**, 1997. Stable isotope studies on Mono Lake (California). 1. $\delta^{18}\text{O}$ in lake sediments as proxy for climatic change during the last 150 years. *Limnology and Oceanography* **42**, 230–238.
- Liu, Z., Yoshimura, K., Bowen, G.J., Buening, N.H., Risi, C., Welker, J.M., Yuan, F.**, 2014. Paired oxygen isotope records reveal modern North

- American atmospheric dynamics during the Holocene. *Nature Communications* 5, 3701.
- Louderback, L.A., Rhode, D.E.**, 2009. 15,000 Years of vegetation change in the Bonneville basin: the Blue Lake pollen record. *Quaternary Science Reviews* 28, 308–326.
- Lund, S., Benson, L., Negrini, R.**, 2021. Timing of Sierra Nevada stadial/interstadial variations from 15 to 56 ka. *Quaternary International* 583, 31–38.
- Lund S.P., Benson L.V.**, 2018. A comparison of western Great Basin paleoclimate records for the last 3000 yr: evidence for multidecadal- to millennial-scale drought. In: Starratt, S.W., Rosen, M.R. (Eds.), *From Saline to Freshwater: The Diversity of Western Lakes in Space and Time. Geological Society of America Special Paper* 536, 183–200.
- Machette, M.N., Personius, S.F., Nelson, A.R., Schwartz, D.P., Lund, W.R.**, 1991. The Wasatch Fault Zone, Utah—segmentation and history of Holocene earthquakes. *Journal of Structural Geology* 13, 137–149.
- Madsen, D.B., Rhode, D., Grayson, D.K., Broughton, J.M., Livingston, S.D., Hunt, J., Quade, J., Schmitt, D.N., Shaver, M.W., III**, 2001. Late Quaternary environmental change in the Bonneville basin, western USA. *Palaeogeography, Palaeoclimatology, Palaeoecology* 167, 243–271.
- Marchetti, D.W., Anderson, L., Donovan, J.J., Harris, M.S., Huth, T.**, 2018. Fish Lake limnology and watershed aqueous geochemistry, Fish Lake Plateau, Utah. In: Emerman, S.H., Bowen, B., Schamel, S., Simmons S. (Eds.), *Geofluids of Utah*. Utah Geological Association Publication 47, pp. 55–74.
- McDonald, G.N., Giraud, R.E.**, 2015. Landslide inventory map for the Upper Muddy Creek Area, Sanpete and Sevier counties, Utah. *Utah Geological Survey Special Study* 155. <https://doi.org/10.34191/SS-155>.
- McGee, D., Quade, J., Edwards, R.L., Broecker, W.S., Cheng, H., Reiners, P.W., Evenson, N.**, 2012. Lacustrine cave carbonates: novel archives of paleohydrologic change in the Bonneville Basin (Utah, USA). *Earth and Planetary Science Letters* 351–352, 182–194.
- Menking, K.M., Bischoff, J.L., Fitzpatrick, J.A., Burdette, J.W., Rye, R.O.**, 1997. Climatic/Hydrologic oscillations since 155,000 yr B.P. at Owens Lake, California, reflected in abundance and stable isotope composition of sediment carbonate. *Quaternary Research* 48, 58–68.
- Mensing, S.A., Sharpe, S.E., Tunno, I., Sada, D.W., Thomas, J.M., Starratt, S., Smith, J.**, 2013. The Late Holocene Dry Period: multiproxy evidence for an extended drought between 2800 and 1850 cal yr BP across the central Great Basin, USA. *Quaternary Science Reviews* 78, 266–282.
- Metcalfe, S.E., Barron, J.A., Davies, S.J.**, 2015. The Holocene history of the North American monsoon: “known knowns” and “known unknowns” in understanding its spatial and temporal complexity. *Quaternary Science Reviews* 120, 1–27.
- Miller W.E.**, 1987. *Mammot americanum*, Utah’s first record of the American mastodon. *Journal of Paleontology* 61, 168–183.
- Mishra, A.K., Singh, V.P.**, 2010. A review of drought concepts. *Journal of Hydrology* 391, 202–216.
- Mock, C.J., Birkeland, K.W.**, 2000. Snow avalanche climatology of the western United States mountain ranges. *Bulletin of the American Meteorological Society* 81, 2367–2392.
- Moore, D.M., Reynolds, R.C., Jr.**, 1989. *X-ray Diffraction and the Identification and Analysis of Clay Minerals*. Oxford University Press, Oxford, 322 pp.
- Morris, J.L., Brunelle, A.R., Munson, A.S.**, 2010. Pollen Evidence of Historical Forest Disturbance on the Wasatch Plateau, Utah. *Western North American Naturalist* 70, 175–188.
- Morris, J.L., DeRose, R.J., Brunelle, A.R.**, 2015. Long-term landscape changes in a subalpine spruce-fir forest in central Utah, USA. *Forest Ecosystems* 2, 35. <https://doi.org/10.1186/s40663-015-0057-0>.
- Munroe, J.S., Bigl, M.F., Silverman, A.E., Laabs, B.J.C.**, 2018. Records of late Quaternary environmental change from high-elevation lakes in the Ruby Mountains and East Humboldt Range, Nevada. In: Starratt, S.W., Rosen, M.R. (Eds.), *From Saline to Freshwater: The Diversity of Western Lakes in Space and Time. Geological Society of America Special Paper* 536, 33–52.
- Munroe, J.S., Laabs, B.J.C.**, 2020. Multiproxy lacustrine records of post-glacial environmental change from the Uinta Mountains, Utah, USA. *Geological Society of America Bulletin* 132, 48–64.
- Oster, J.L., Kelley, N.P.**, 2016. Tracking regional and global teleconnections recorded by western North American speleothem records. *Quaternary Science Reviews* 149, 18–33.
- Oviatt, C.G.**, 2015. Chronology of Lake Bonneville, 30,000 to 10,000 yr B.P. *Quaternary Science Reviews* 110, 166–171.
- Pederson, G.T., Gray, S.T., Woodhouse, C.A., Betancourt, J.L.**, 2011. The unusual nature of recent snowpack declines in the North America Cordillera. *Science* 333, 332–335.
- PRISM Climate Group**, 2018. *PRISM Climate Data*. <https://prism.oregonstate.edu>. [accessed 2018-Jan-26]
- Quirk, B.J., Moore, J.R., Laabs, B.J.C., Plummer, M.A., Caffee, M.W.**, 2020. Latest Pleistocene glacial and climate history of the Wasatch Range, Utah. *Quaternary Science Reviews* 238, 106313. <https://doi.org/10.1016/j.quascirev.2020.106313>.
- Redmond, K.T.**, 2003. Climate variability in the west: complex spatial structure associated with topography and observational issues. In: Lewis, W.M., Jr. (Ed.), *Water and Climate in the Western United States*. Boulder, Colorado, University Press of Colorado, pp. 29–48.
- Reheis, M.C., Adams, K.D., Oviatt, C.G., Bacon, S.N.**, 2014. Pluvial lakes in the Great Basin of the western United States—a view from the outcrop. *Quaternary Science Reviews* 97, 33–57.
- Routson, C.C., Woodhouse, C.A., Overpeck, J.T.**, 2011. Second century megadrought in the Rio Grande headwaters, Colorado: how unusual was medieval drought? *Geophysical Research Letters* 38, L22703. <https://doi.org/10.1029/2011GL050015>.
- Shapley, M.D., Finney, B.P., Krueger, C.R.**, 2021. Characteristics of landslide-formed lakes of central Idaho: High-resolution archives of watershed productivity and clastic sediment delivery. In: Starratt, S.W., Rosen, M.R. (Eds.), *From Saline to Freshwater: The Diversity of Western Lakes in Space and Time. Geological Society of America Special Paper* 536, 241–258.
- Shapley, M.D., Ito, E., Donovan, J.J.**, 2005. Authigenic calcium carbonate flux in groundwater-controlled lakes: implications for lacustrine paleoclimate records. *Geochimica et Cosmochimica Acta* 69, 2517–2533.
- Shapley, M.D., Ito, E., Donovan, J.J.**, 2008. Isotopic evolution and climate paleorecords: modeling boundary effects in groundwater-dominated lakes. *Journal of Paleolimnology* 39, 17–33.
- Shapley, M.D., Ito, E., Donovan, J.J.**, 2009. Lateglacial and Holocene hydroclimate inferred from a groundwater flow-through lake, Northern Rocky Mountains, U.S.A. *The Holocene* 19, 523–535.
- Shinker, J.J., Bartlein, P.J.**, 2011. Spatial variations of effective moisture in the western U.S. *Geophysical Research Letters* 37, L02701. <https://doi.org/10.1029/2009GL041387>.
- Shinker, J.J., Bartlein, P.J., Shuman, B.**, 2006. Synoptic and dynamic climate controls of North American mid-continental aridity. *Quaternary Science Reviews* 25, 1401–1417.
- Shuman, B.N., Carter, G.E., Hougardy, D.D., Powers, K., Shinker, J.J.**, 2014. A north-south moisture dipole at multi-century scales in the central and southern Rocky Mountains, U.S.A., during the Late Holocene. *Rocky Mountain Geology* 49(1), 33–49.
- Shurtliff, R.A., Nelson, S.T., McBride, J.H., Rey, K.A., Tucker, J.C., Godwin, S.B., Tingey, D.G.**, 2017. A 13 000 year multi-proxy climate record from central Utah (western USA), emphasizing conditions leading to large mass movements. *Boreas* 46(2), 308–324.
- Sjostrom, D.J., Hren, M.T., Chamberlain, C.P.**, 2004. Oxygen isotope records of goethite from ferricrete deposits indicate regionally varying holocene climate change in the Rocky Mountain region, U.S.A. *Quaternary Research* 61, 64–71.
- Smith, A.J., Palmer, D.F.**, 2012. The versatility of Quaternary ostracods as palaeoclimate proxies. In: Horne, D.J., Holmes, J., Rodriguez-Lazaro, J., Viehberg, F. (Eds.), *Ostracoda as Proxies for Quaternary Climate Change. Developments in Quaternary Sciences Vol. 17*. Elsevier, Amsterdam, pp. 183–203.
- Smith, G.I.**, 2002. Stable isotope compositions of waters in the Great Basin, United States 3. Comparison of groundwaters with modern precipitation. *Journal of Geophysical Research* 107(D19), 4402. <https://doi.org/10.1029/2001JD000567>.
- Spieker, E.M., Billings, M.P.**, 1940. Glaciation in the Wasatch Plateau, Utah. *Geological Society of America Bulletin* 51, 1173–1197.
- Steinman, B., Abbott, M.B., Mann, M.E., Ortiz, J.D., Feng, S., Pompeani, D.P., Stansell, N.D., Anderson, L., Finney, B.P., Bird, B.W.**, 2014.

- Ocean-atmosphere forcing of centennial hydroclimate variability in the Pacific Northwest. *Geophysical Research Letters* **41**, 2553–2560.
- Stefonaitis, E., Andrews, A., McGee, D., Quade, J., Hsieh, Y.-T., Broecker, W.S., Shuman, B.N., Burns, S.J., Cheng, H.**, 2015. Mid-Holocene drying of the U.S. Great Basin recorded in Nevada speleothems. *Quaternary Science Reviews* **127**, 174–185.
- Stevens, L.R., Dean, W.E.**, 2008. Geochemical evidence for hydroclimatic variability over the last 2460 years from Crevice Lake in Yellowstone National Park, U.S.A. *Quaternary International* **188**, 139–148.
- Stevens, L.R., Stone, J.R., Campbell, J., Fritz, S.C.**, 2006. A 2200-yr record of hydrologic variability from Foy Lake, Montana, USA, inferred from diatom and geochemical data. *Quaternary Research* **65**, 264–274.
- Stone, J.R., Saros, J.E., Pederson, G.T.**, 2016. Coherent late-Holocene climate-driven shifts in the structure of three Rocky Mountain lakes. *The Holocene* **26**, 1103–1111.
- Stuiver, M., Reimer, P.J., Reimer, R.W.**, 2021. *Calib 8.2*. <http://calib.org>. [accessed 2021-Mar-3]
- Talbot, M.R.**, 1990. A review of the palaeohydrological interpretation of carbon and oxygen isotopic ratios in primary lacustrine carbonates. *Chemical Geology (Isotope Geosciences Section)* **80**, 261–279.
- Tarutani, T., Clayton, R.N., Mayeda, T.K.**, 1969. The effect of polymorphism and magnesium substitution on oxygen isotope fractionation between calcium carbonate and water. *Geochimica et Cosmochimica Acta* **33**, 987–996.
- Theissen, K.M., Hickson, T.A., Brundrett, A.L., Horns, S.E., Lachniet, M.S.**, 2019. A record of mid- and Late Holocene paleohydroclimate from Lower Pahranaagat Lake, southern Great Basin. *Quaternary Research* **92**, 352–364.
- Thompson, R.S., Oviatt, C.G., Honke, J.S., McGeehin, J.P.**, 2016. Late Quaternary changes in lakes, vegetation, and climate in the Bonneville Basin reconstructed from sediment cores from Great Salt Lake. In: Oviatt, C.G., Shroder, J.F. (Eds.), *Lake Bonneville: A Scientific Update. Developments in Earth Surface Processes Vol. 20*. Elsevier, Amsterdam, pp. 221–291.
- Thompson, R.S., Whitlock, C., Bartlein, P.J., Harrison, S.P., Spaulding, W.G.**, 1993. Climatic changes in the western United States since 18,000 yr B.P. In: Wright, H.E., Jr., Kutzbach, J.E., Webb, T., III, Ruddiman, W.F., Street-Perrott, F.A., Bartlein, P.J. (Eds.), *Global Climates Since the Last Glacial Maximum*. University of Minnesota Press, Minneapolis, pp. 468–513.
- Wahl, D., Starratt, S., Anderson, L., Kusler, J., Fuller, C., Addison, J., Wan, E.**, 2015. Holocene environmental changes inferred from biological and sedimentological proxies in a high elevation Great Basin lake in the northern Ruby Mountains, Nevada, USA. *Quaternary International* **387**, 87–98.
- Weber, M., Hinz, Y., Schöne, B.R., Jochum, K.P., Hoffmann, D., Spötl, C., Riechelmann, D.F.C., Scholz, D.**, 2021. Opposite trends in Holocene speleothem proxy records from two neighboring caves in Germany: a multi-proxy evaluation. *Frontiers in Earth Science* **9**. <https://www.frontiersin.org/article/10.3389/feart.2021.642651>.
- Whitlock, C., Dean, W.E., Fritz, S.C., Stevens, L.R., Stone, J.R., Power, M.J., Rosenbaum, J., Pierce, K.L., Bracht-Flyer, B.**, 2012. Holocene seasonal variability inferred from multiple proxy records from Crevice Lake, Yellowstone National Park, USA. *Palaeogeography, Palaeoclimatology, Palaeoecology* **331–332**, 90–103.
- Witkind, I.J., Weiss, M.P., Brown, T.L.**, 2006. Geologic map of the Manti 30' x 60' quadrangle, Carbon, Emery, Juab, SanPete, and Sevier counties, Utah. *Utah Geological Survey Map 212DM* (digitized from U.S. Geological Survey Miscellaneous Investigations Series Map I-1631 [1987]). <https://ugspub.nr.utah.gov/publications/geologicmaps/30x60quadrangles/m-212.pdf>.
- Wittkop, C.A., Teranes, J.L., Dean, W.E., Guilderson, T.P.**, 2009. A lacustrine carbonate record of Holocene seasonality and climate. *Geology* **37**, 695–698.
- Yuan, F., Koran, M.R., Valdez, A.**, 2013. Late glacial and Holocene records of climatic change in the southern Rocky Mountains from sediments in San Luis Lakes, Colorado USA. *Palaeogeography, Palaeoclimatology, Palaeoecology* **392**, 146–160.
- Zimmerman, S.R.H., Wahl, D.B.**, 2020. Holocene paleoclimate change in the western US: The importance of chronology in discerning patterns and drivers. *Quaternary Science Reviews* **246**, 106487. <https://doi.org/10.1016/j.quascirev.2020.106487>.